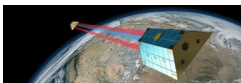# Precise Orbit Determination

Adrian Jäggi

Astronomical Institute

University of Bern
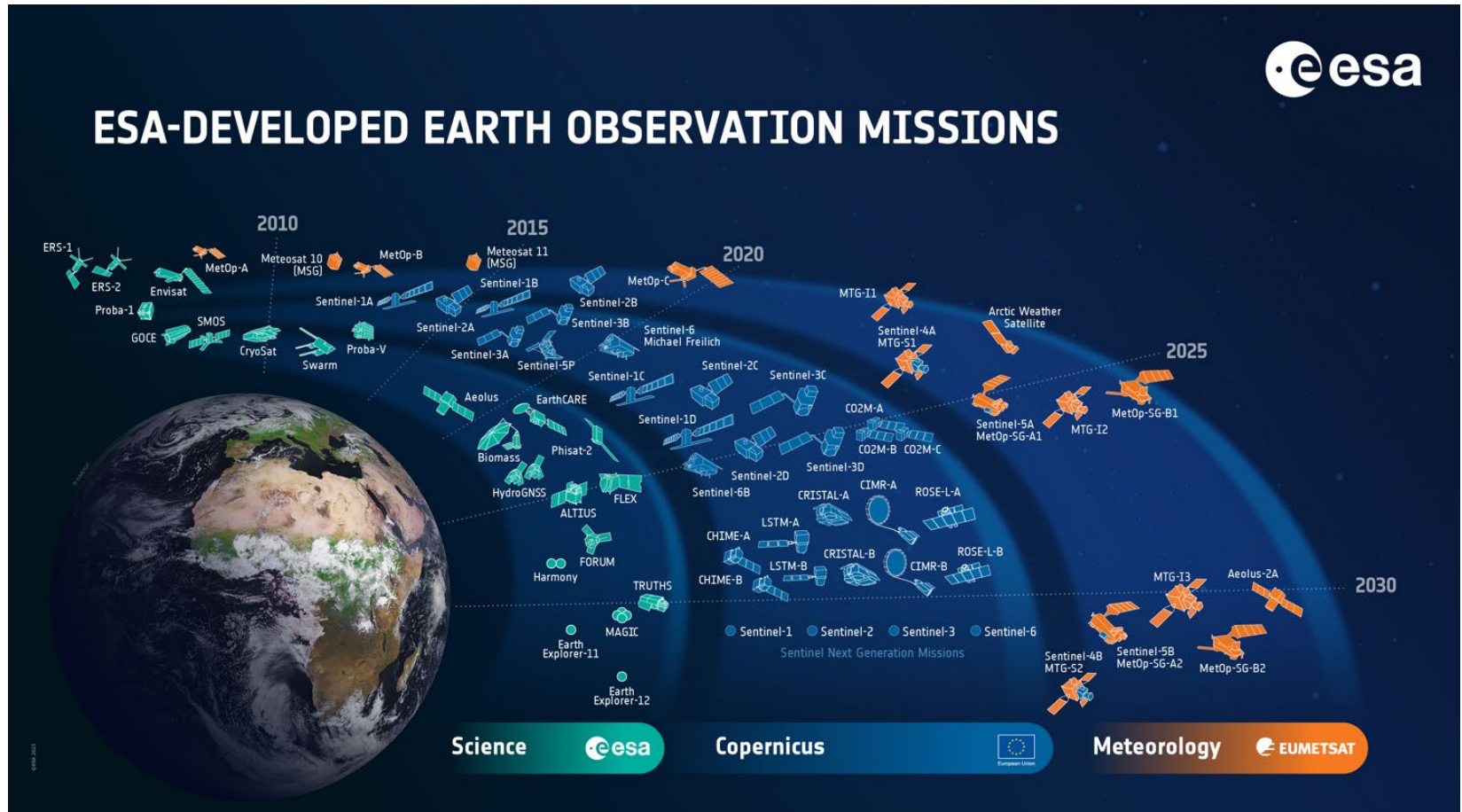
Lecture Contents
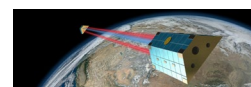
1. Introduction

2. Global Positioning System

3. Different Orbit Representations

4. Principles of Orbit Determination

5. GPS-based LEO POD
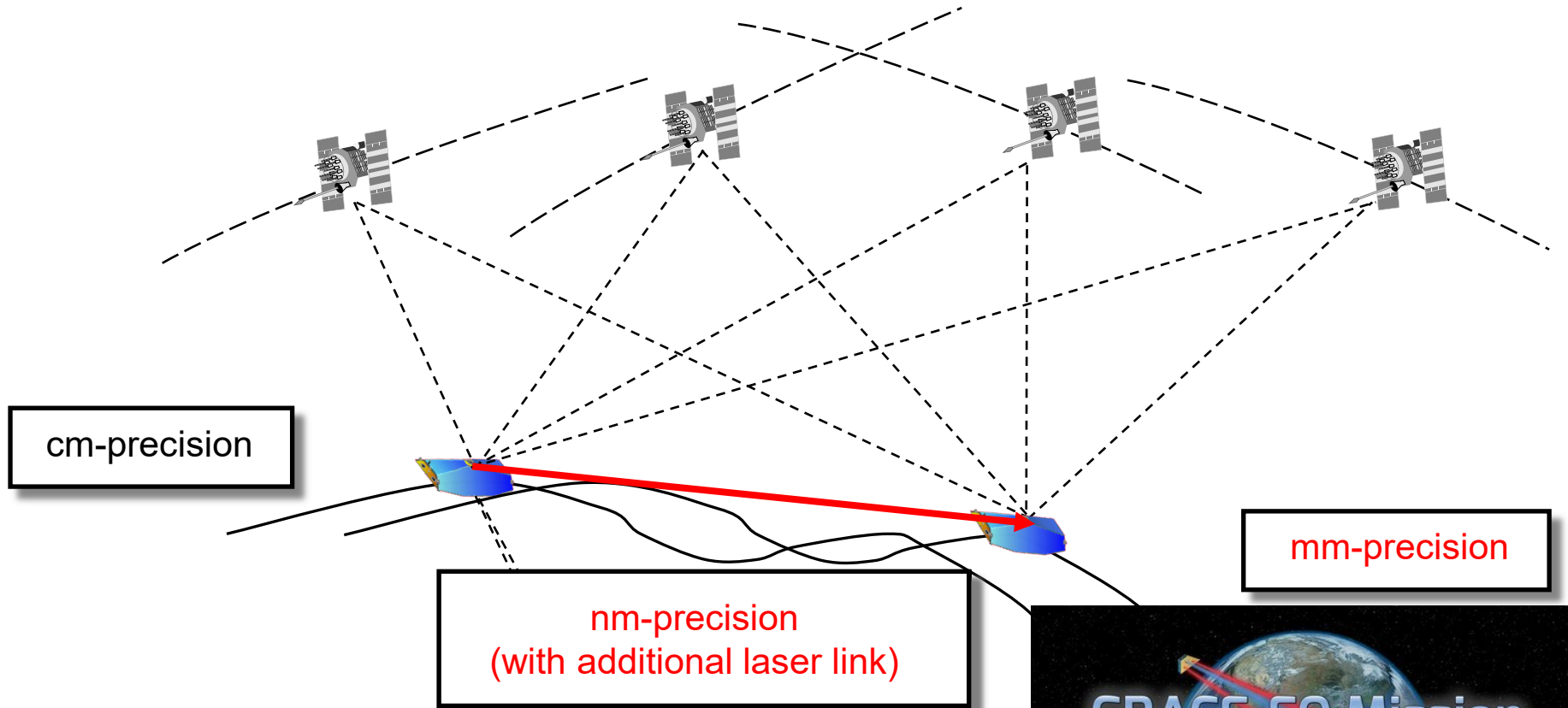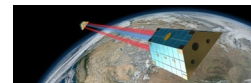
6. Orbit Validation
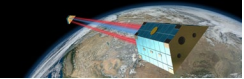
A multitude of Earth Observation Satellites

Courtesy: ESA

Precise Tracking Data in Near Earth Space

cm-precision

mm-precision

nm-precision
(with additional laser link)

GRACE-FO Mission

LISA Technology
Sheds Light on Climate Change

Low Earth Orbiters (LEOs)

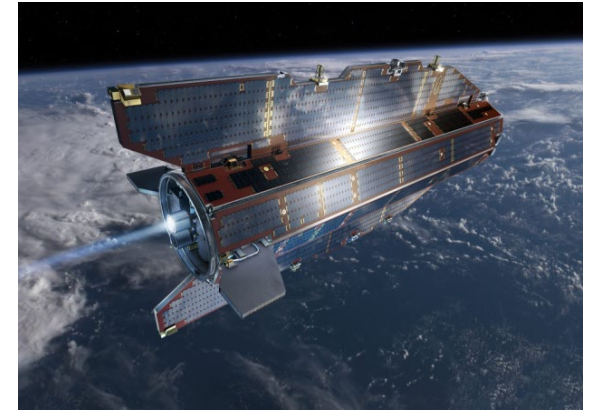| **CHAMP**	**GRACE**	**GOCE**
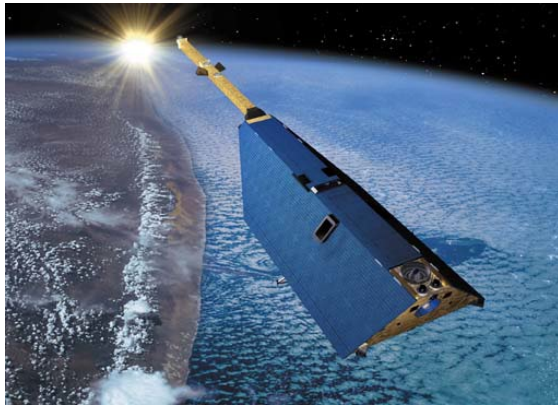
CHAllenging
Minisatellite **P**ayload
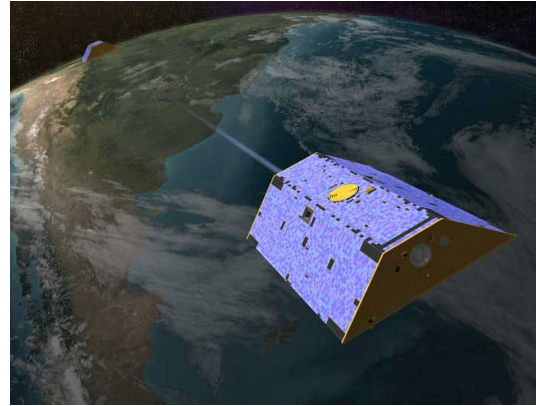
Gravity **R**ecovery **A**nd
Climate **E**xperiment

Gravity and
steady-state **O**cean
Circulation **E**xplorer

Of course, there are many more missions equipped with GPS receivers

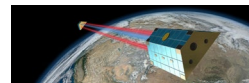| Jason	Jason-2	MetOp-A	Icesat	COSMIC

u^b

UNIVERSITÄT
BERN

AIUB
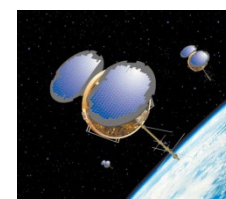
LEO Constellations

TanDEM-X

Swarm

Sentinel

GRACE-FO

GRACE-FO Mission

LISA Technology
Sheds Light on Climate Change

COSMIC-2

LEO CubeSats

Spire

e.g.

~ 150 Spire satellites are already
in different orbits, offering dual-
frequency high-quality GPS data
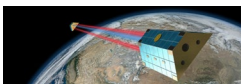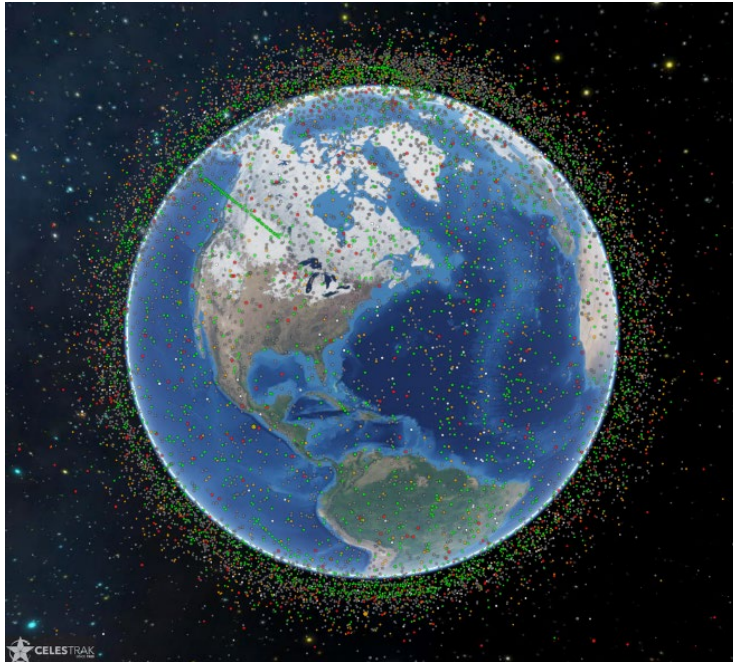
A multitude of **CubeSats** already
exist or are planned for the future

Many more will follow …
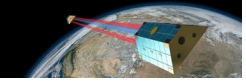
Global Positioning System

Introduction to GPS

GPS

Galileo

visible sat = 12

Empfangene Satelliten :10
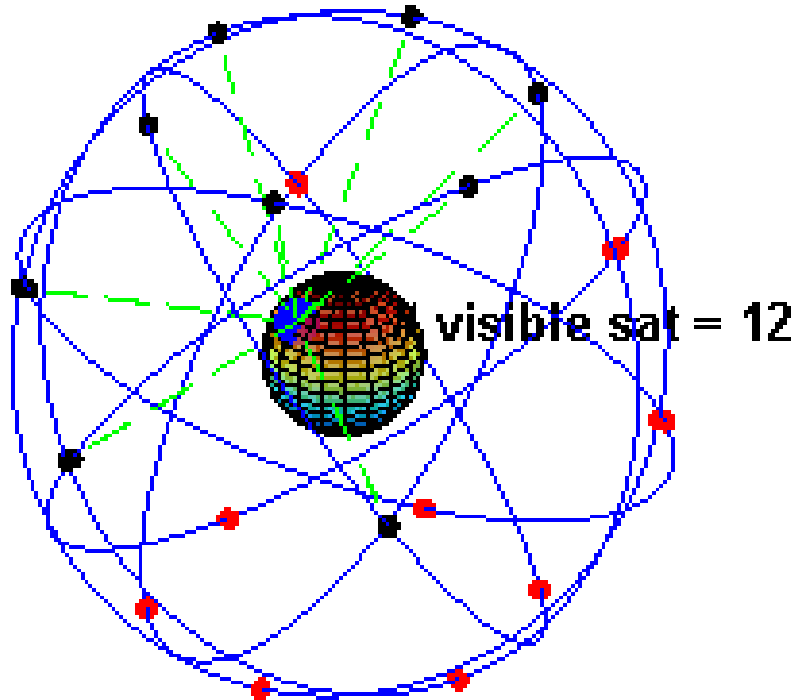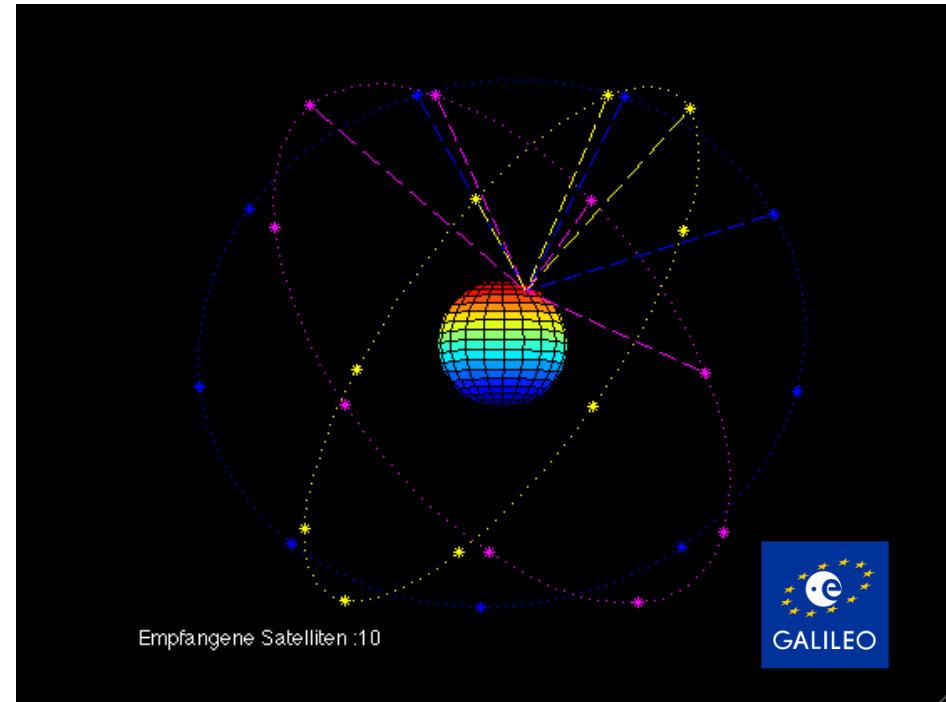
GALILEO

Other **Global Navigation Satellite Systems** (GNSS) are also available (GLONASS, Galileo, Beidou), but for a long time no multi-GNSS spaceborne receivers were in orbit. This changed with the launches of Fengyun-3, COSMIC-2, Sentinel-6.

AIUB

u^b

UNIVERSITÄT
BERN
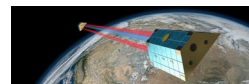
Introduction to GPS

GPS: **G**lobal **P**ositioning **S**ystem

Characteristics:

- Satellite system for (real-time) **Positioning** and **Navigation**

- **Global** (everywhere on Earth, up to altitudes of 5000km) and **at any time**

- **Unlimited** number of users

- **Weather-independent** (radio signals are passing through the atmosphere)

- **3-dimensional position**, **velocity** and **time** information

AIUB

u^b
UNIVERSITÄT
BERN

GPS Segments

The GPS consists of **3 main segments**:

- **Space Segment**: the satellites and the constellation of satellites

- **Control Segment**: the ground stations, infrastructure and software for operation and monitoring of the GPS

- **User Segment**: all GPS receivers worldwide and the corresponding processing software
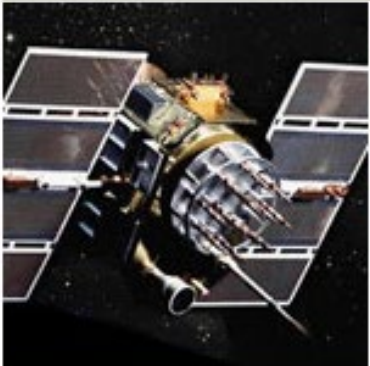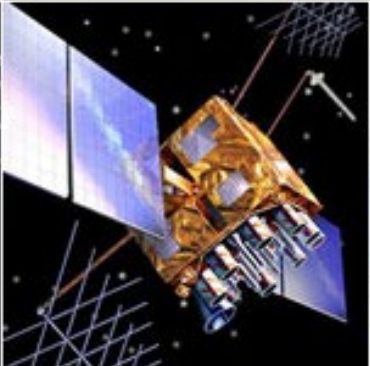
We should add an important **4th segment**:

- **Ground Segment**: all civilian permanent networks of reference sites and the international/regional/local services delivering products for the users

AIUB

u^b

UNIVERSITÄT
BERN
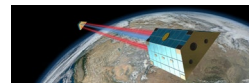
Space Segment

- The space segment nominally consists of **24 satellites**, presently: 31 active GPS satellites

- Constellation design: at least **4 satellites** in view from **any location** on the Earth at **any time**

LEGACY SATELLITES		MODERNIZED SATELLITES		
BLOCK IIA	BLOCK IIR	BLOCK IIR-M	BLOCK IIF	GPS III/IIIF
0 operational	6 operational	7 operational	12 operational	6 operational

https://www.gps.gov/systems/gps/space/

AIUB

u^b

UNIVERSITÄT BERN
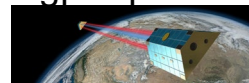
Global Network of the IGS

★ GNSS
● GPS only
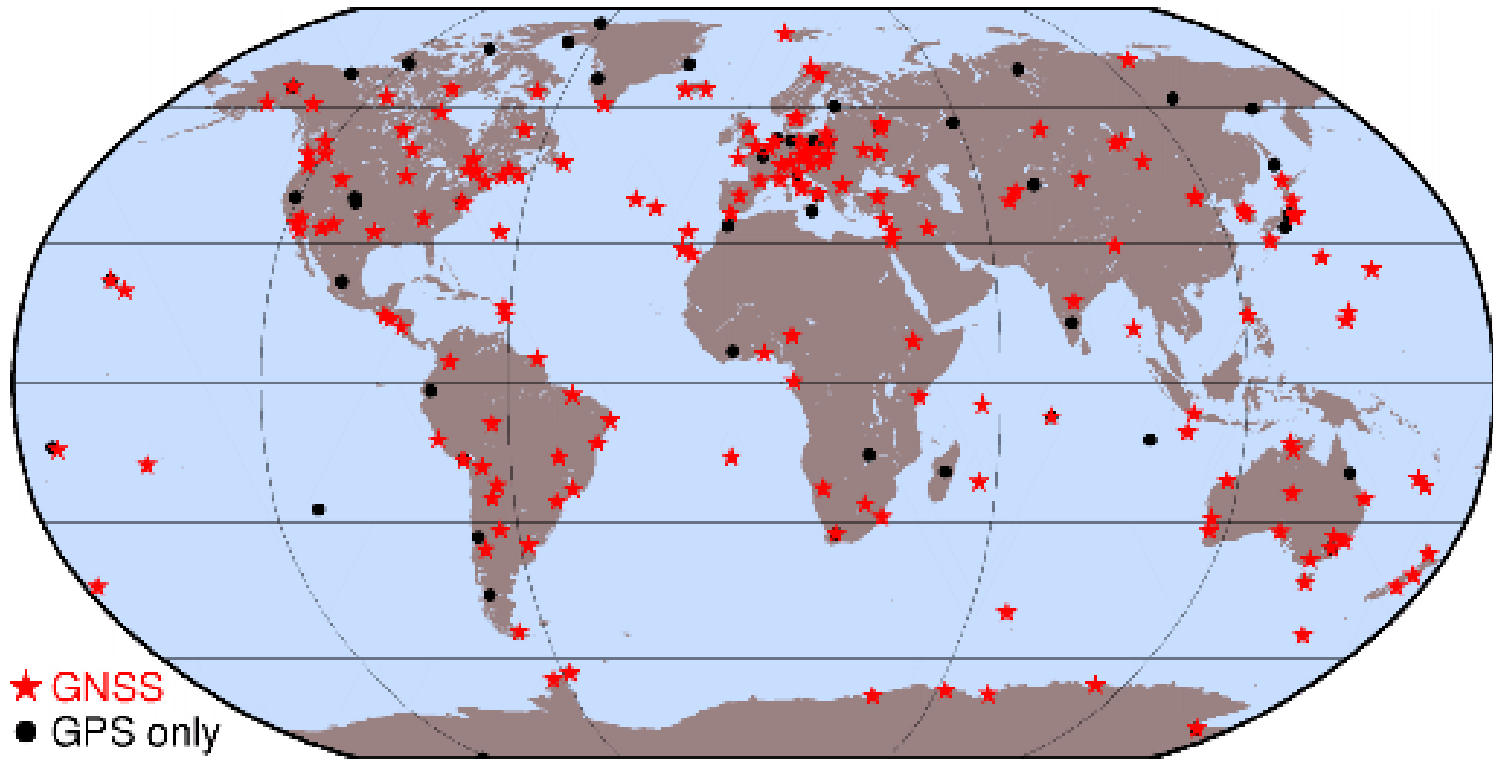
IGS stations used for computation of final orbits at CODE (Dach et al., 2009)

AIUB

u^b
UNIVERSITÄT
BERN

Performance of IGS Final Orbits

Final Orbits (AC solutions compared to IGS Final)

http://acc.igs.org/
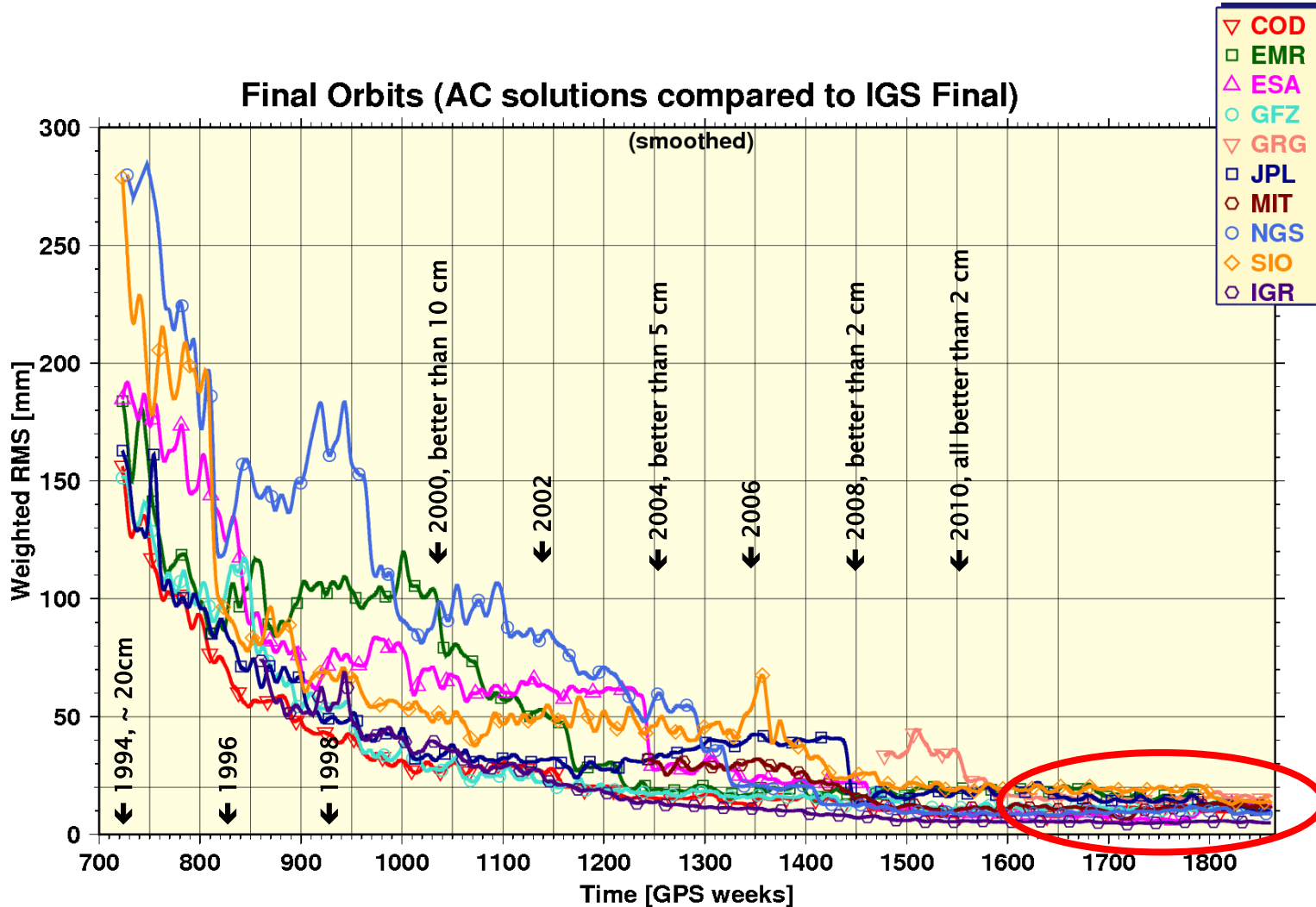
Computation of High-Rate Clocks

Pre-processing	Clean code + phase Smooth code	⇐ RINEX 30 s and 5 s
Screening of post-fit residuals	Screening station-by-station Delete bad stations 1. Phase only 2. code only 3. phase + code	⇐ CODE Rapid solution CRD TRP PRE ERP CLK
Low-rate clock solution	**3 global clusters** 40 stations/cluster Combination + merging **=> 5-min clocks**	⇐ CODE Final solution CRD TRP PRE ERP
High-rate clock solutions	EHRI from 5 min to 30 s EHRI from 30 s to 5 s	⇐ CRD and TRP for remaining 5-s stations

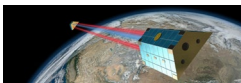(Bock et al., 2009)

The final clock product with 5 min sampling is based on undifferenced GPS data of typically 120 stations of the IGS network

The IGS 1 Hz network is finally used for clock densification to 5 sec

The 5 sec clocks are interpolated to 1 sec as needed for 1 Hz kinematic LEO POD

AIUB

u^b
UNIVERSITÄT
BERN

GPS Signals
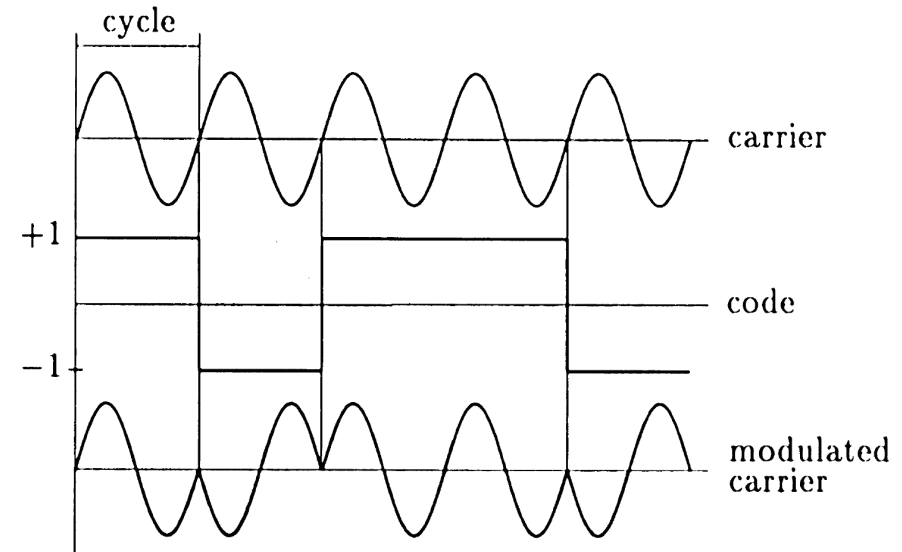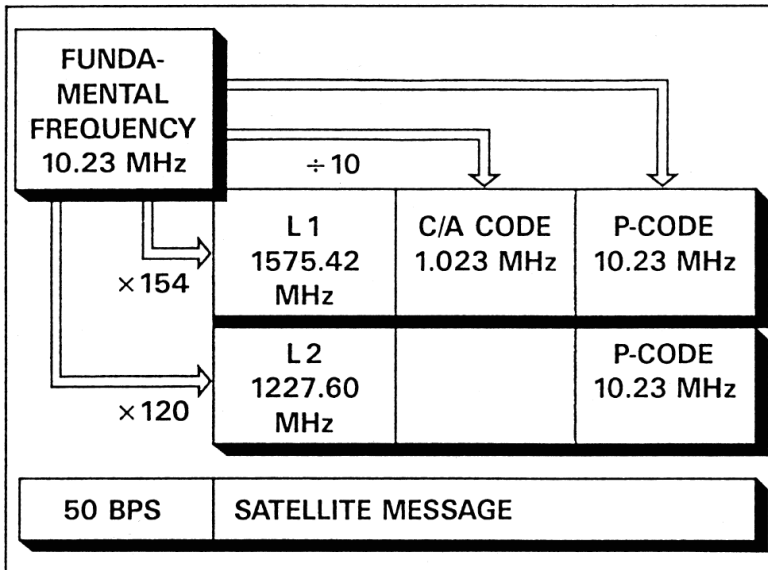
Bits encoded on carrier by phase modulation:

Signals driven by an **atomic clock**

Two **carrier signals** (sine waves):

- **L1**: f = 1575.43 MHz, λ = 19 cm
- **L2**: f = 1227.60 MHz, λ = 24 cm

- **C/A-code** (Clear Access / Coarse Acquisition)
- **P-code** (Protected / Precise)
- **Broadcast/Navigation Message**
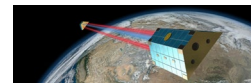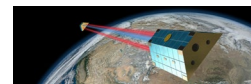
Pseudorange / Code Measurements

Code Observations P_i^k are defined as:

$$P_i^k \doteq c \left(T_i - T^k \right)$$

c Spee

T_i Recei

T^k GPS   ne)

- No actual „**range**" (distance) because of clock offsets

- **Measurement noise**: ~ 0.5 m for P-code   (Blewitt, 1997)

(Teunissen & Montenbruck, 2017)
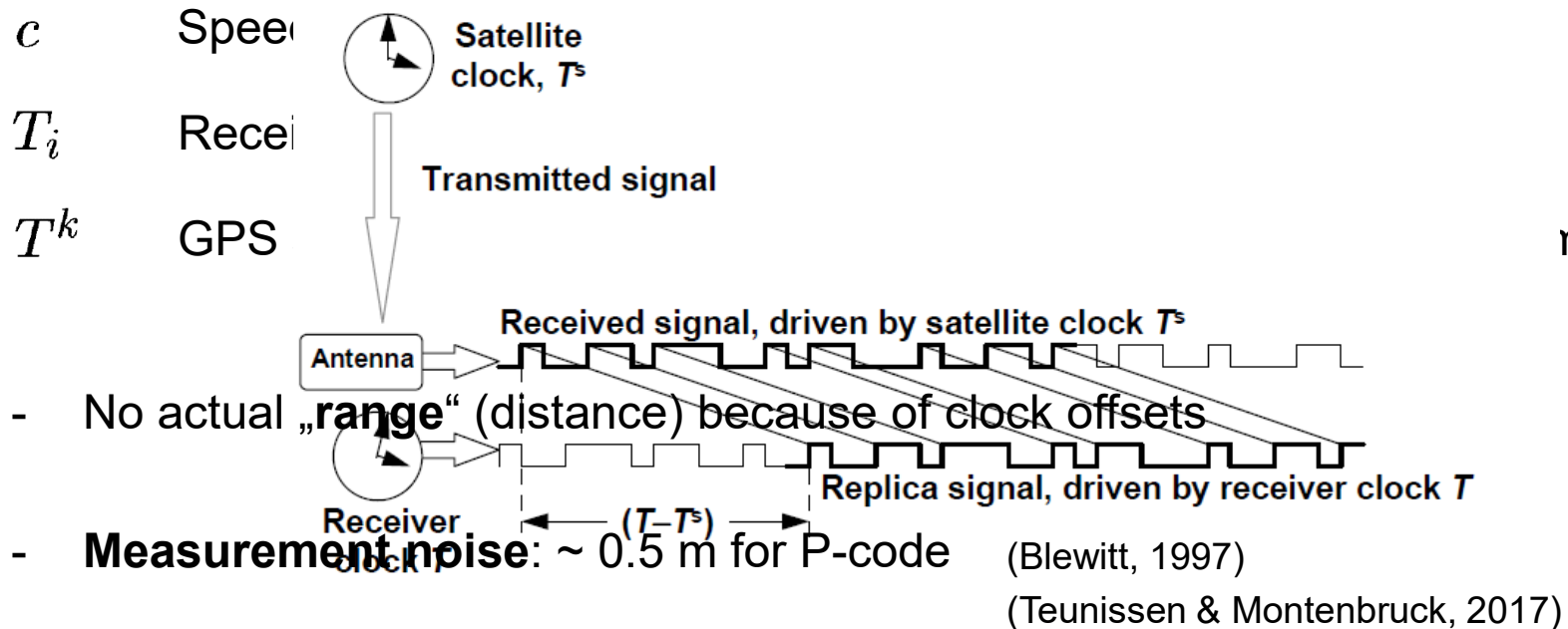
Code Observation Equation

$$P_i^k = \rho_i^k - c \cdot \Delta t^k + c \cdot \Delta t_i$$

t_i, t^k GPS time of reception and emission

Δt^k Satellite clock offset $T^k - t^k$

Δt_i Receiver clock offset $T_i - t_i$

ρ_i^k Distance between receiver and satellite $c\,(t_i - t^k)$

Known from ACs or IGS:

- satellite positions $(x^{k_j}, y^{k_j}, z^{k_j})$

- satellite clock offsets Δt^{k_j}

4 unknown parameters:

- receiver position (x_i, y_i, z_i)

- receiver clock offset Δt_i

AIUB

u^b

UNIVERSITÄT
BERN

Carrier Phase Measurements (1)
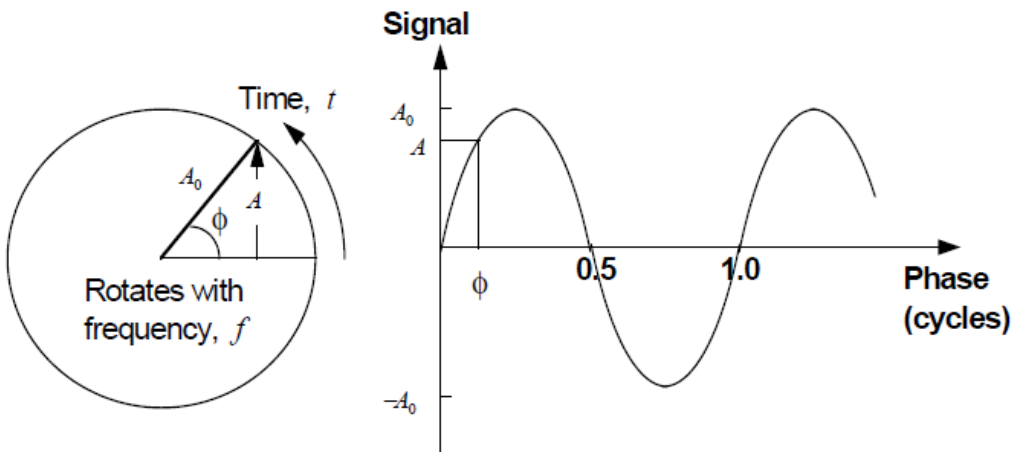
Phase ϕ (in cycles) increases linearly with time t :

$$\phi = f \cdot t$$

where f is the frequency

The **satellite** generates with its clock the phase signal ϕ^k. At emission time T^k (in satellite clock time) we have
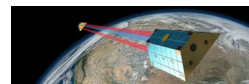
$$\phi^k = f \cdot T^k$$

The same phase signal, e.g., a wave crest, propagates from the satellite to the receiver, but the receiver measures only the fractional part of the phase and does not know the **integer number of cycles** N_i^k (phase ambiguity):

$$\phi_i^k = \phi^k - N_i^k = f \cdot T^k - N_i^k$$
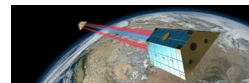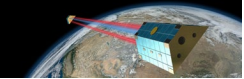
Carrier Phase Measurements (2)

The **receiver** generates with its clock a **reference phase**. At time of reception T_i of the satellite phase ϕ_i^k (in receiver clock time) we have:

$$\phi_i = f \cdot T_i$$

The actual **phase measurement** is the difference between receiver reference phase ϕ_i and satellite phase ϕ_i^k:

$$\psi_i^k = \phi_i - \phi_i^k = f \cdot T_i - (f \cdot T^k - N_i^k) = f \cdot (T_i - T^k) + N_i^k$$

Multiplication with the wavelength $\lambda = c/f$ leads to the **phase observation equation** in meters:

$$L_i^k = \lambda \cdot \psi_i^k = c \cdot (T_i - T^k) + \lambda \cdot N_i^k$$
$$= \rho_i^k - c \cdot \Delta t^k + c \cdot \Delta t_i + \lambda \cdot N_i^k$$

Difference to the pseudorange observation: **integer ambiguity term** N_i^k

u^b

UNIVERSITÄT
BERN

AIUB
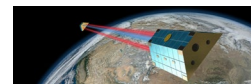
Detailed Observation Equation

$$L_i^k = \rho_i^k - c \cdot \Delta t^k + c \cdot \Delta t_i + \cancel{T_i^k} + \cancel{I_i^k} + \lambda \cdot N_i^k$$

$$+ \Delta_{rel} - c \cdot b^k + c \cdot b_i + m_i^k + \epsilon_i^k$$

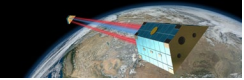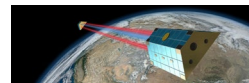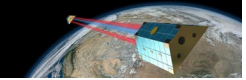|		
ρ_i^k	Distance between satellite and receiver ⬅	Satellite positions and clocks
Δt^k	Satellite clock offset wrt GPS time ⬅	are known from the IGS
Δt_i	Receiver clock offset wrt GPS time	
~~T_i^k~~	~~Tropospheric delay~~ ⬅	Not existent for LEOs
~~I_i^k~~	~~Ionospheric delay~~ ⬅	Cancels out (first order only)
N_i^k	Phase ambiguity	when forming the ionosphere-
Δ_{rel}	Relativistic corrections	free linear combination:
b^k	Delays in satellite (cables, electronics)	
b_i	Delays in receiver and antenna	$L_c = \dfrac{f_1^2}{f_1^2 - f_2^2} L_1 - \dfrac{f_2^2}{f_1^2 - f_2^2} L_2$
m_i^k	Multipath, scattering, bending effects	
ϵ_i^k	Measurement error	

Geometric Distance

Geometric distance ρ_{leo}^k is given by:

$$\rho_{leo}^k = |\boldsymbol{r}_{leo}(t_{leo}) - \boldsymbol{r}^k(t_{leo} - \tau_{leo}^k)|$$

$\boldsymbol{r}_{leo}$ Inertial position of LEO antenna phase center at reception time

$\boldsymbol{r}^k$ Inertial position of GPS antenna phase center of satellite k at emission time

τ_{leo}^k Signal traveling time between the two phase center positions

Different ways to represent $\boldsymbol{r}_{leo}$:

- **Kinematic** orbit representation

- **Dynamic** or **reduced-dynamic** orbit representation

AIUB

$\boldsymbol{u}^b$

UNIVERSITÄT
BERN

Different Orbit Representations

Kinematic Orbit Representation (1)

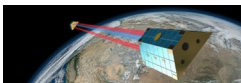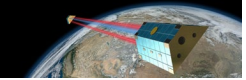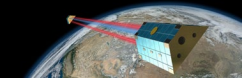**Satellite position** $r_{leo}(t_{leo})$ (in inertial frame) is given by:

$$r_{leo}(t_{leo}) = R(t_{leo}) \cdot (r_{leo,e,0}(t_{leo}) + \delta r_{leo,e,ant}(t_{leo}))$$
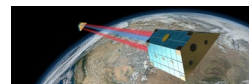
R Transformation matrix from Earth-fixed to inertial frame

$r_{leo,e,0}$ LEO center of mass position in Earth-fixed frame

$\delta r_{leo,e,ant}$ LEO antenna phase center offset in Earth-fixed frame

Kinematic positions $r_{leo,e,0}$ are estimated for each **measurement epoch**:

- Measurement epochs **need not** to be identical with nominal epochs

- Positions are **independent** of models describing the LEO dynamics.
  Velocities and accelerations cannot be provided in a "strict" sense.

u^b

UNIVERSITÄT
BERN

AIUB

Kinematic Orbit Representation (2)
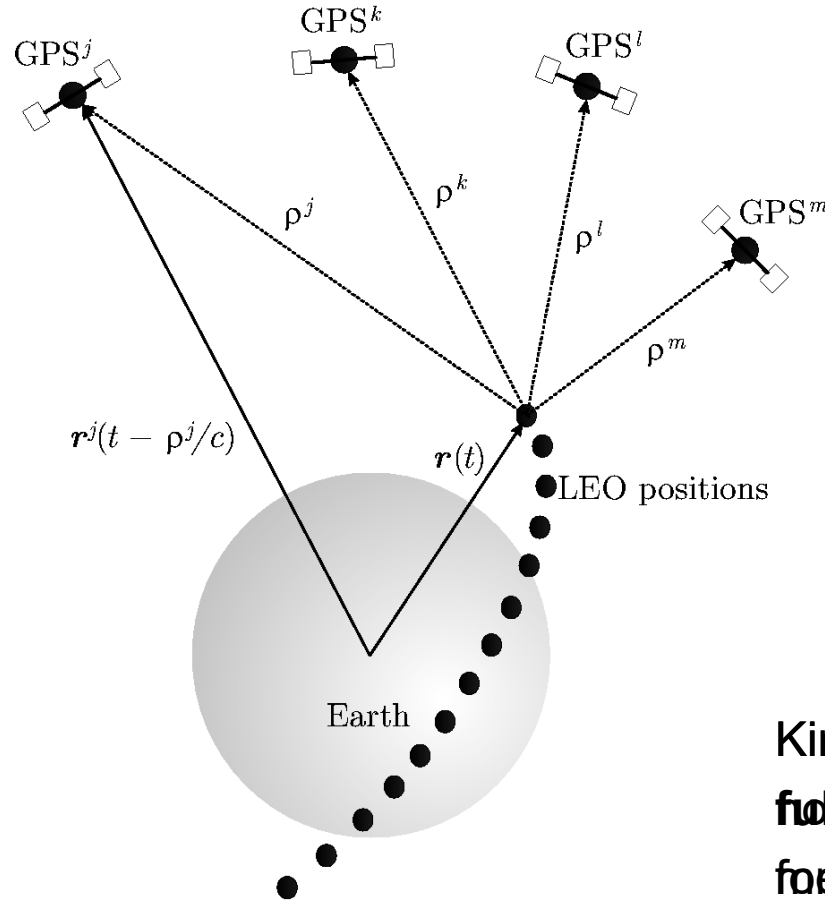
A kinematic orbit is an ephemeris at **discrete** measurement epochs

Kinematic positions are fully independent from the force models used (LEO orbit determination) (Švehla and Rothacher, 2004)

Kinematic Orbit Representation (3)

Measurement epochs
(in GPS time)

Positions (km)
(Earth-fixed)

Clock correction to nominal epoch (μs), e.g., to epoch 00:00:03

```
*    2009 11  2   0   0   0.80678020
PL15    -390.612059      6623.987679      73.104149   193219.797196
*    2009 11  2   0   0   1.80678020
PL15    -389.240315      6624.166512      65.402457   193219.799413
*    2009 11  2   0   0   2.80678020
PL15    -387.868014      6624.336133      57.700679   193219.801634
*    2009 11  2   0   0   3.80678020
PL15    -386.495163      6624.496541      49.998817   193219.803855
*    2009 11  2   0   0   4.80678019
PL15    -385.121760      6624.647724      42.296889   193219.806059
*    2009 11  2   0   0   5.80678019
PL15    -383.747819      6624.789703      34.594896   193219.808280
*    2009 11  2   0   0   6.80678019
PL15    -382.373332      6624.922464      26.892861   193219.810495
*    2009 11  2   0   0   7.80678019
PL15    -380.998306      6625.046003      19.190792   193219.812692
*    2009 11  2   0   0   8.80678019
PL15    -379.622745      6625.160329      11.488692   193219.814899
*    2009 11  2   0   0   9.80678018
PL15    -378.246651      6625.265448       3.786580   193219.817123
```

Excerpt of kinematic GOCE positions at begin of 2 Nov, 2009
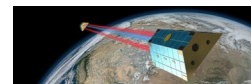
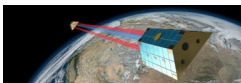# Recovery of Large-Scale Time-Variable Gravity Signals
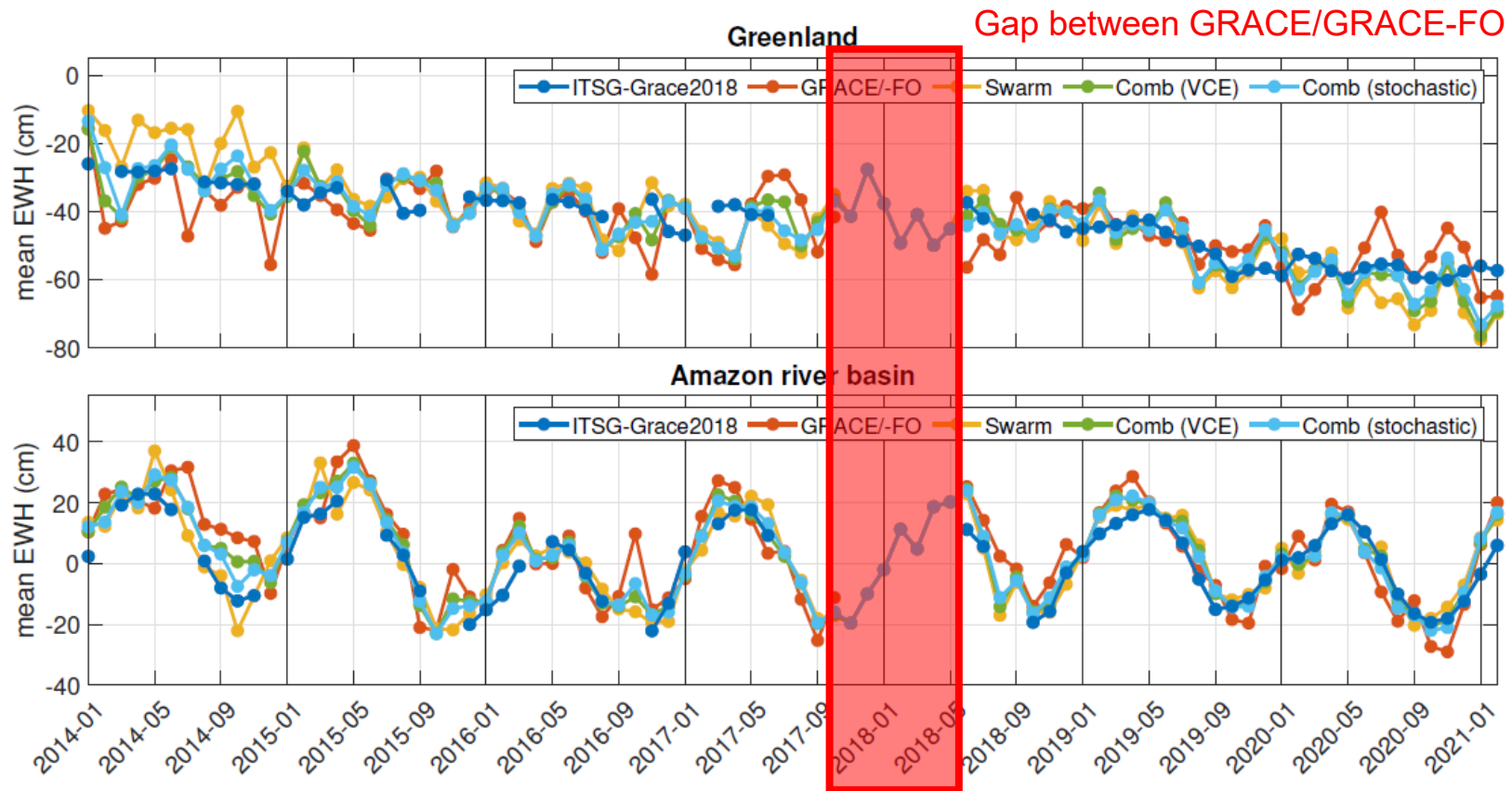
Kinematic positions allow it to recover the **long wavelength** part of the Earth's time-variable gravity field. The scatter of monthly gravity field solutions is larger than from dedicated GRACE/GRACE-FO data, but trends and annual signals may be derived remarkably well.
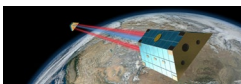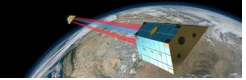
(Grombein et al., 2022)
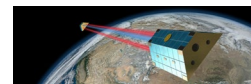
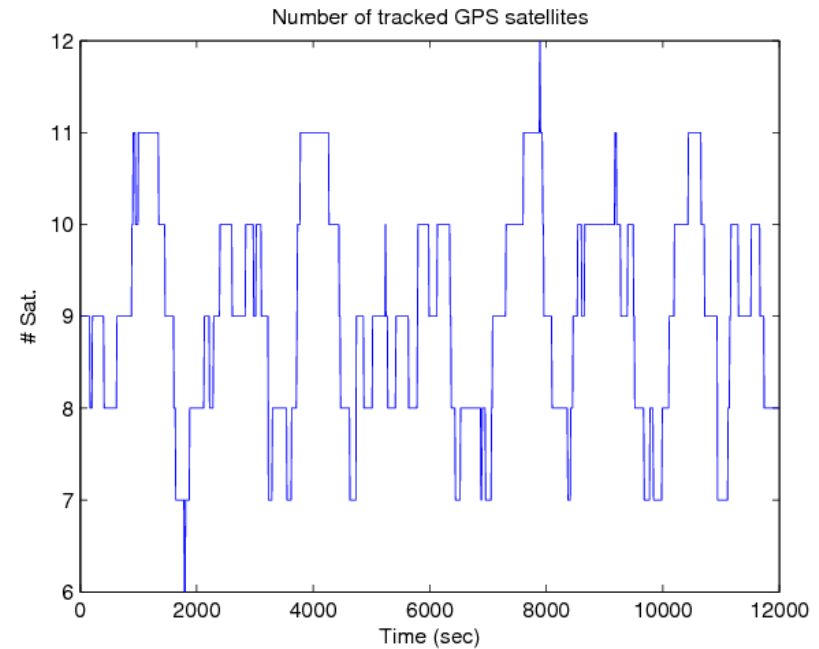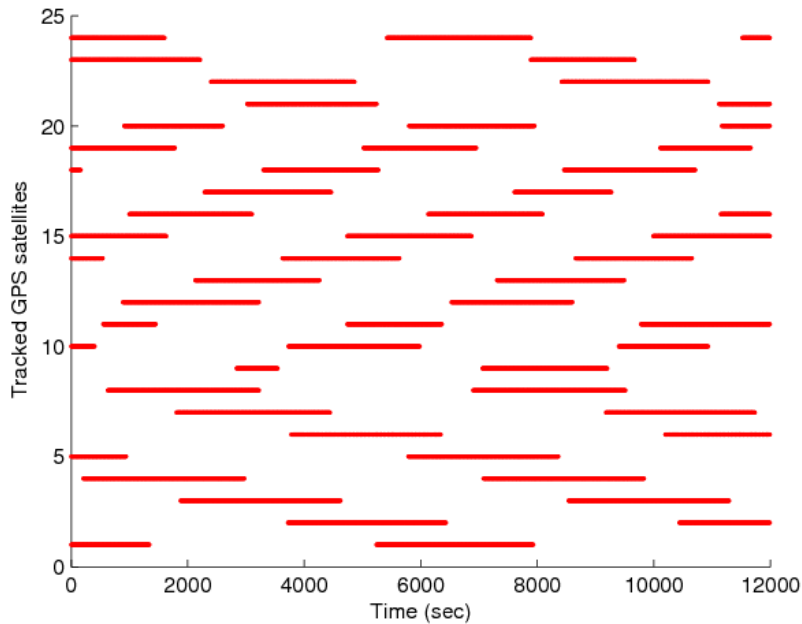# Example: Sentinel-3A GPS Tracking
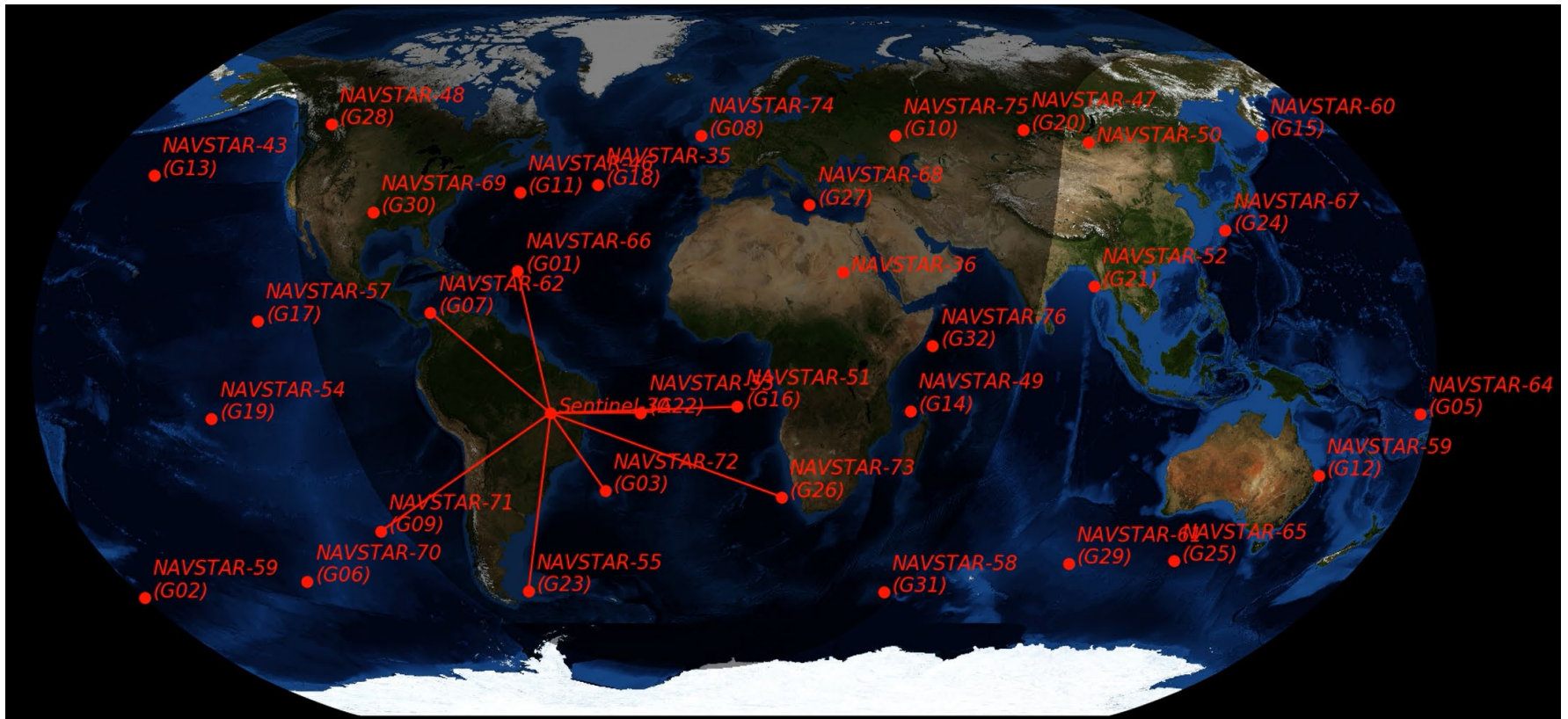
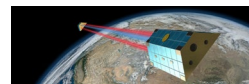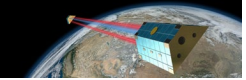# Example: Sentinel-6A multi-GNSS Tracking

GPS Satellite Visibility

Tracking scenario of a simulated data set (left). Up to 12 GPS satellites are at maximum simultaneously visible from the LEO satellite (right). The viewing geometry is continuously changing due to the orbital motion of all satellites.
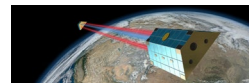
Dynamic Orbit Representation (1)

Satellite position $r_{leo}(t_{leo})$ (in inertial frame) is given by:

$$r_{leo}(t_{leo}) = r_{leo,0}(t_{leo}; a, e, i, \Omega, \omega, u_0; Q_1, ..., Q_d) + \delta r_{leo,ant}(t_{leo})$$

$r_{leo,0}$	LEO center of mass position
$\delta r_{leo,ant}$	LEO antenna phase center offset
$a, e, i, \Omega, \omega, u_0$	LEO initial osculating orbital elements
$Q_1, ..., Q_d$	LEO dynamical parameters

Satellite trajectory $r_{leo,0}$ is a particular solution of an **equation of motion**

- One set of **initial conditions** (orbital elements) is estimated per arc.
  Dynamical parameters of the force model may be estimated on request.

u^b

UNIVERSITÄT
BERN

AIUB

Dynamic Orbit Representation (2)

Equation of motion (in inertial frame) is given by:

$$\ddot{\boldsymbol{r}} = -GM\frac{\boldsymbol{r}}{r^3} + \boldsymbol{f}_1(t, \boldsymbol{r}, \dot{\boldsymbol{r}}, Q_1, ..., Q_d)$$

with initial conditions
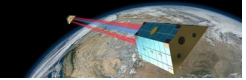
$$\boldsymbol{r}(t_0) = \boldsymbol{r}(a, e, i, \Omega, \omega, u_0; t_0)$$
$$\dot{\boldsymbol{r}}(t_0) = \dot{\boldsymbol{r}}(a, e, i, \Omega, \omega, u_0; t_0)$$

The **acceleration** $\boldsymbol{f}_1$ consists of **gravitational** and **non-gravitational** perturbations taken into account to model the satellite trajectory. Unknown parameters $Q_1, ..., Q_d$ of force models may appear in the equation of motion together with deterministic (known) accelerations given by analytical models.

AIUB

$\boldsymbol{u}^b$

UNIVERSITÄT
BERN

Perturbing Accelerations of a LEO Satellite

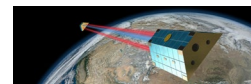| Force	Acceleration (m/s²)
Central term of Earth's gravity field	8.42
Oblateness of Earth's gravity field	0.015
Atmospheric drag	0.00000079
Higher order terms of Earth's gravity field	0.00025
Attraction from the Moon	0.0000054
Attraction from the Sun	0.0000005
Direct solar radiation pressure	0.000000097
...	...

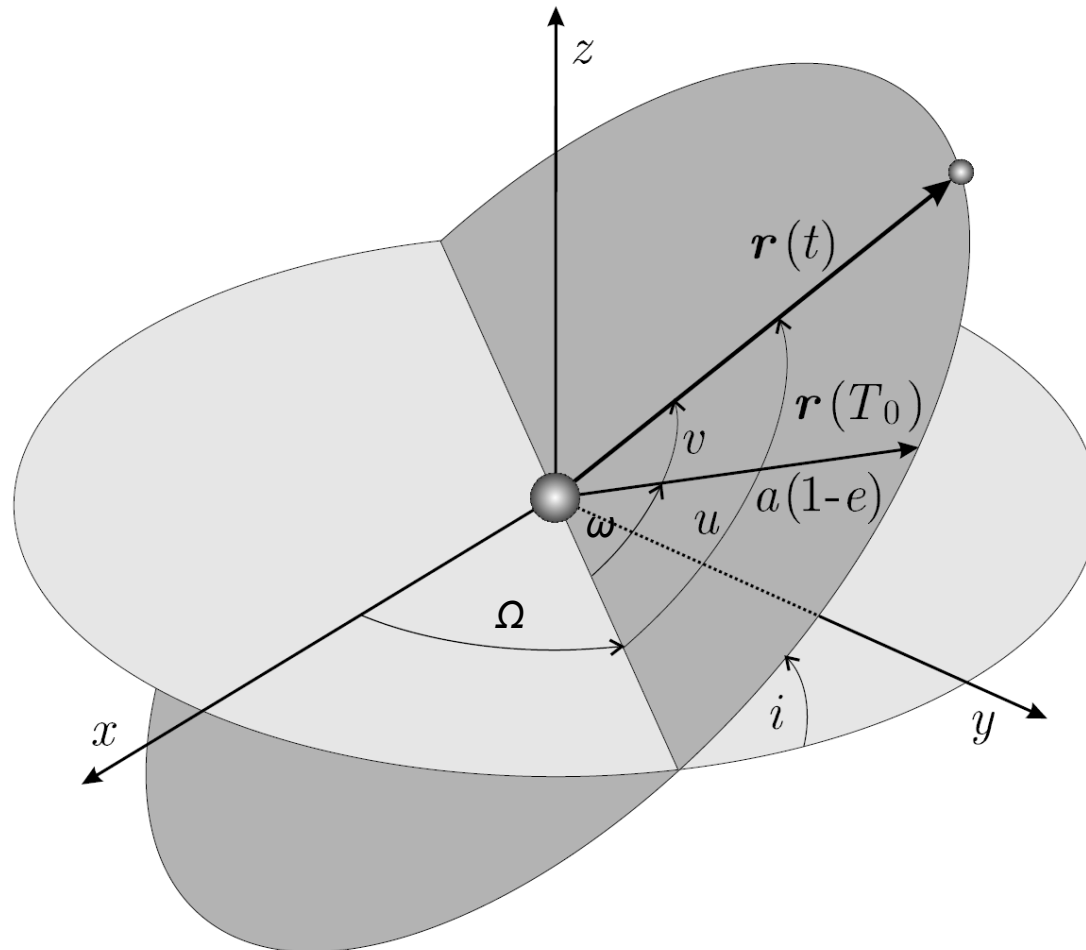# Perturbing Accelerations of a LEO Satellite
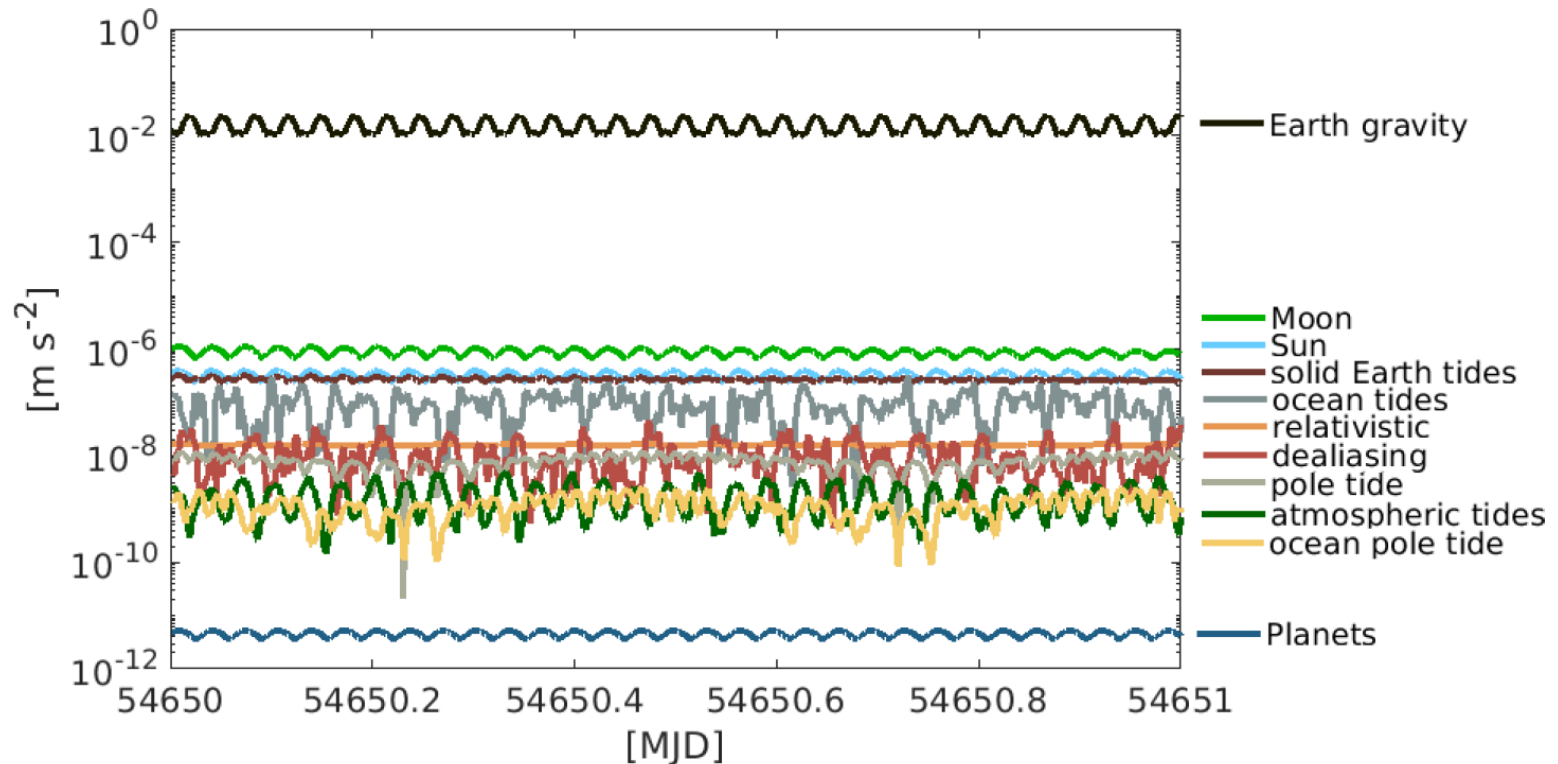
Norm of the **COST-G benchmark accelerations** along a GRACE satellite orbit. The benchmark data set may be used as a reference data set and provides the opportunity to test the implementation of corresponding background models.

(Mayer-Gürr and Kvas, 2019; Lasser et al., 2020)
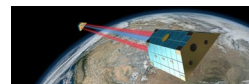
Osculating Orbital Elements

(Beutler, 2005)

Osculating Orbital Elements of GOCE (1)
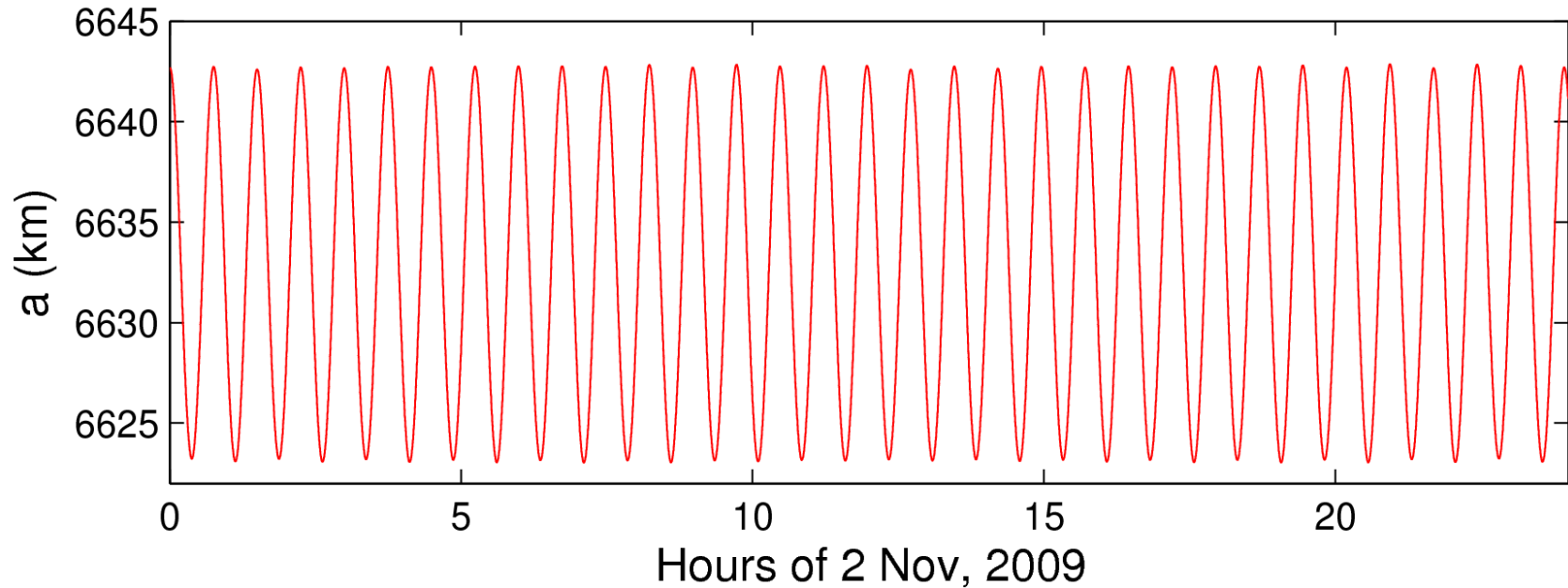
Semi-major axis:

Twice-per-revolution variations of about ±10 km around the mean semi-major axis of 6632.9km, which corresponds to a mean altitude of 254.9 km

Osculating Orbital Elements of GOCE (2)
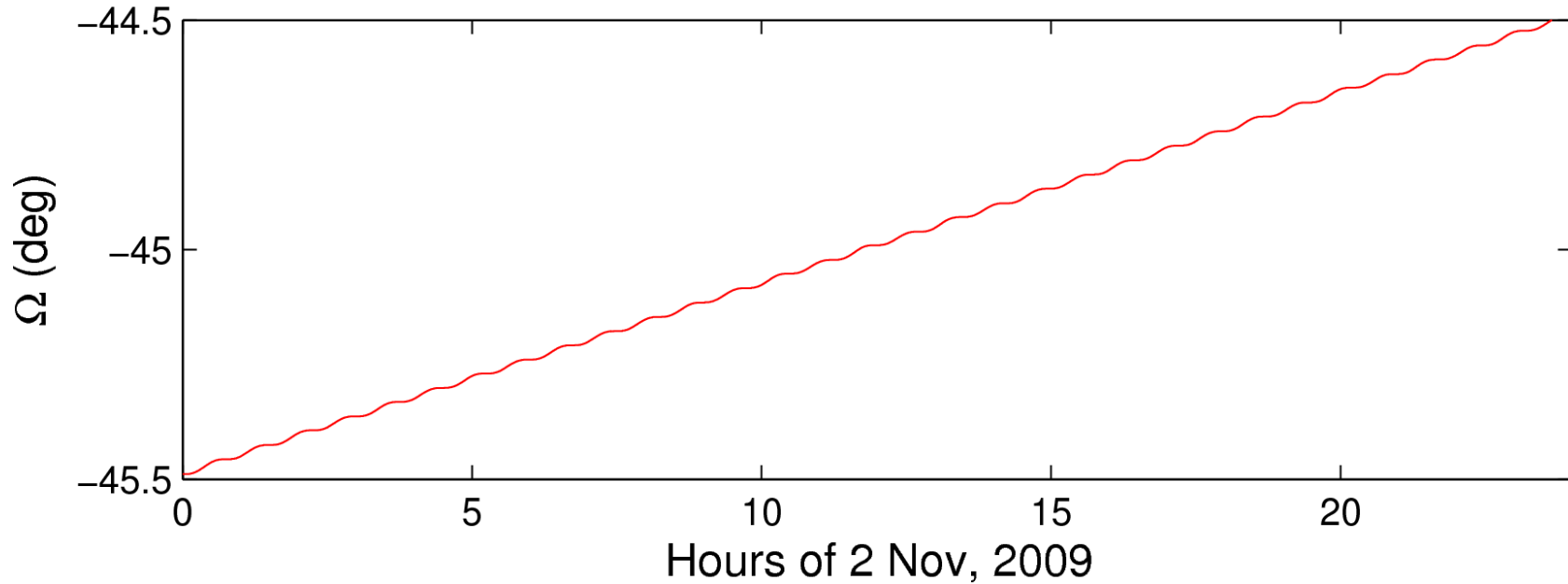
Right ascension of ascending node:

Twice-per-revolution variations and linear drift of about +1°/day (360°/365days) due to the sun-synchronous orbit

Dynamic Orbit Representation (3)
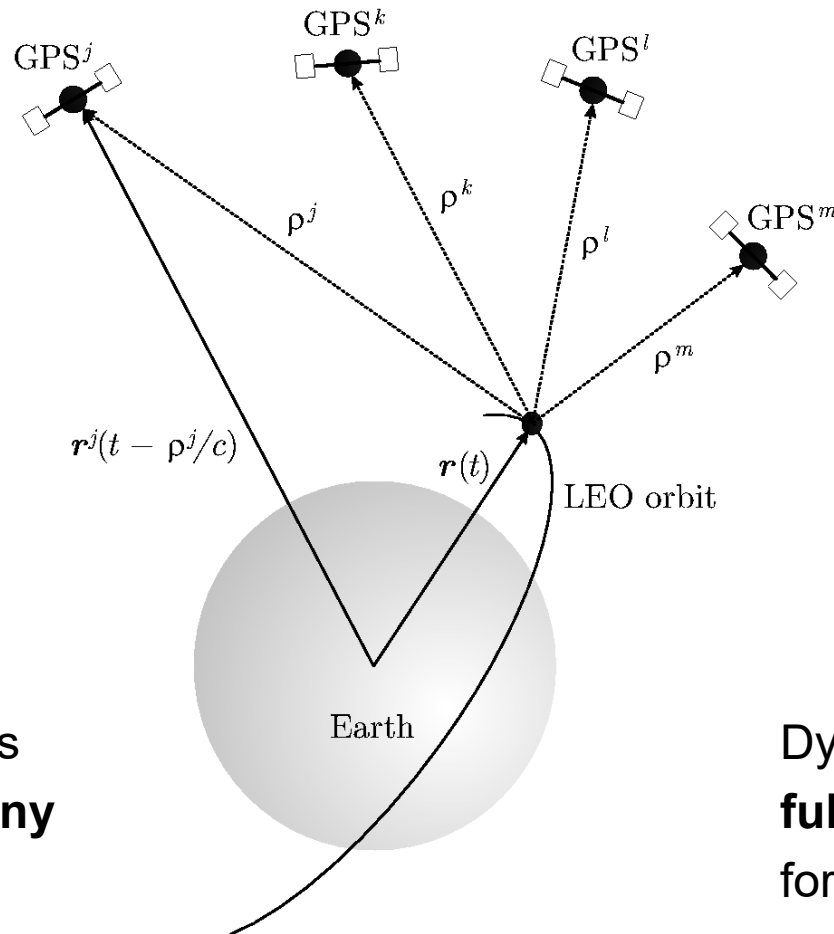
Dynamic orbit positions may be computed at **any epoch** within the arc

Dynamic positions are **fully dependent** on the force models used, e.g., on the gravity field model
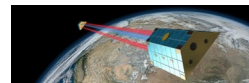
Reduced-Dynamic Orbit Representation (1)

Equation of motion (in inertial frame) is given by:

$$\ddot{\boldsymbol{r}} = -GM\frac{\boldsymbol{r}}{r^3} + \boldsymbol{f}_1(t, \boldsymbol{r}, \dot{\boldsymbol{r}}, Q_1, ..., Q_d, P_1, ..., P_s)$$

$$P_1, ..., P_s \qquad \text{Pseudo-stochastic parameters}$$

Pseudo-stochastic parameters are:

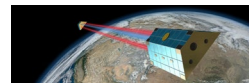- additional empirical parameters characterized by a priori known **statistical properties**, e.g., by expectation values and a priori variances

- useful to **compensate** for deficiencies in dynamic models, e.g., deficiencies in models describing non-gravitational accelerations

- often set up as **piecewise constant accelerations** to ensure that satellite trajectories are continuous and differentiable at any epoch

$$\boldsymbol{u}^b$$

AIUB

UNIVERSITÄT
BERN

Reduced-Dynamic Orbit Representation (2)
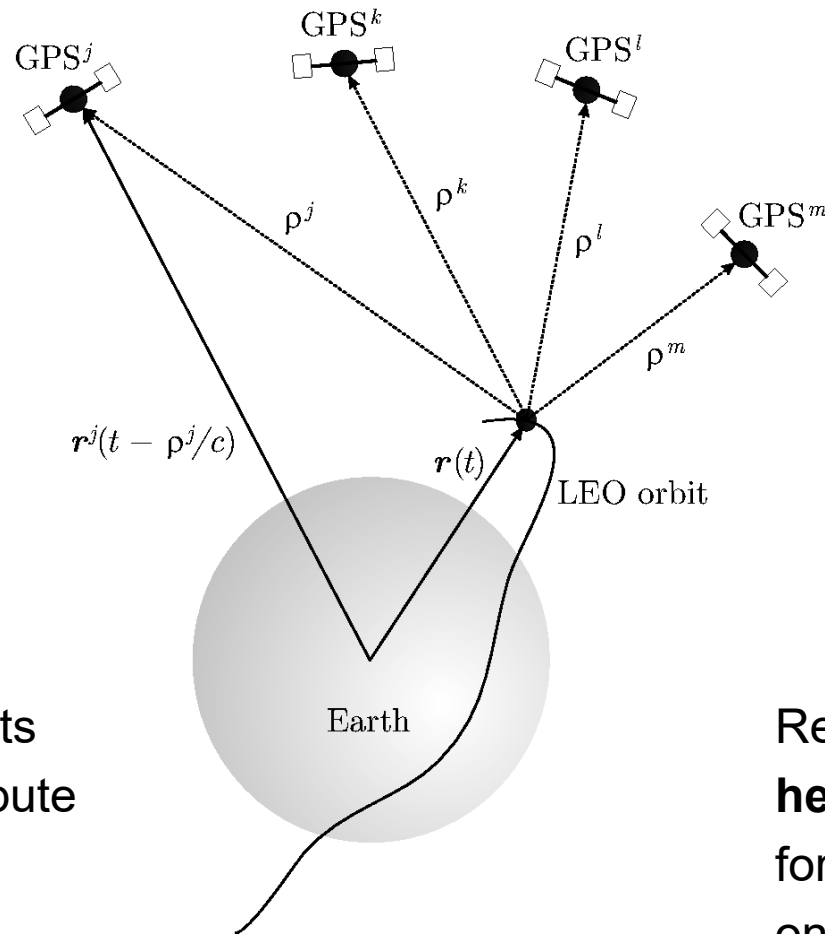
Reduced-dynamic orbits are well suited to compute LEO orbits of **highest quality**

(Jäggi et al., 2006; Jäggi, 2007)

Reduced-dynamic orbits **heavily depend** on the force models used, e.g., on the gravity field model

AIUB

u^b

UNIVERSITÄT
BERN

Reduced-dynamic Orbit Representation (3)

Position epochs
(in GPS time)

Positions (km) &
Velocities (dm/s)
(Earth-fixed)

Clock corrections
are not provided

```
*   2009 11   2    0    0   0.00000000
PL15    -391.718353      6623.836682        79.317661   999999.999999
VL15   13710.157683      1908.731015    -77015.601314   999999.999999
*   2009 11   2    0    0  10.00000000
PL15    -377.980705      6625.284690         2.298385   999999.999999
VL15   13764.602016       987.250587    -77021.193676   999999.999999
*   2009 11   2    0    0  20.00000000
PL15    -364.190222      6625.811136       -74.721213   999999.999999
VL15   13815.825127        65.631014    -77016.232293   999999.999999
*   2009 11   2    0    0  30.00000000
PL15    -350.350131      6625.415949      -151.730567   999999.999999
VL15   13863.820409      -855.995477    -77000.719734   999999.999999
*   2009 11   2    0    0  40.00000000
PL15    -336.463660      6624.099187      -228.719134   999999.999999
VL15   13908.581905     -1777.497047    -76974.660058   999999.999999
*   2009 11   2    0    0  50.00000000
PL15    -322.534047      6621.861041      -305.676371   999999.999999
VL15   13950.104280     -2698.741871    -76938.058807   999999.999999
*   2009 11   2    0    1   0.00000000
PL15    -308.564533      6618.701833      -382.591743   999999.999999
VL15   13988.382807     -3619.598277    -76890.923043   999999.999999
```
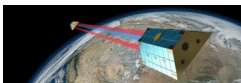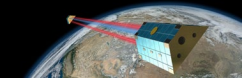
Excerpt of reduced-dynamic GOCE positions at begin of 2 Nov, 2009
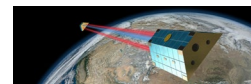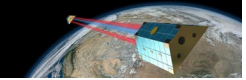
Principles of Orbit Determination

Principle of Orbit Determination

The **actual orbit** $r(t)$ is expressed as a truncated Taylor series:

$$r(t) = r_0(t) + \sum_{i=1}^{n} \frac{\partial r_0}{\partial P_i}(t) \cdot (P_i - P_{0,i})$$

$r_0(t)$ A priori orbit

$\dfrac{\partial r_0}{\partial P_i}(t)$ Partial derivative of the a priori orbit $r_0(t)$ w.r.t. parameter P_i
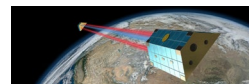
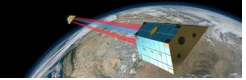$P_{0,i}$ A priori parameter values of the a priori orbit $r_0(t)$

P_i Parameter values of the improved orbit $r(t)$

A **least-squares** adjustment of spacecraft tracking data yields **corrections** to the a priori parameter values $P_{0,i}$. Using the above equation, the improved (linearized) orbit $r(t)$ may be eventually computed.

AIUB

u^b

UNIVERSITÄT
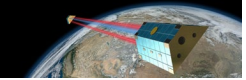BERN

Numerical Integration (1)

Collocation algorithms (one particular class of numerical integration techniques) are subsequently used to briefly illustrate the principles of numerical integration:
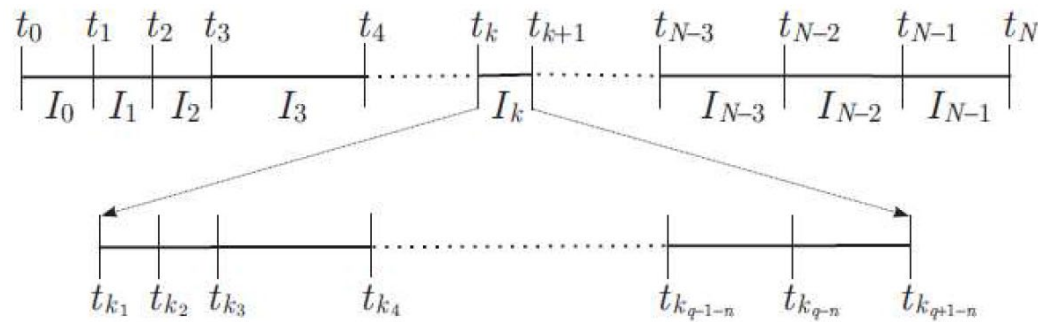
The original intervall is divided into N integration intervals. For each interval I_k a further subdivision is performed according to the order q of the adopted method. At these points t_{k_j} the numerical solution is requested to solve the differential equation system of order n.

(Beutler, 2005)
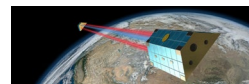
Numerical Integration (2)

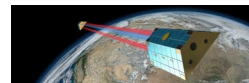**Initial value problem** in the interval I_k is given by:

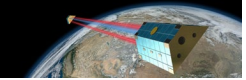$$\ddot{\mathbf{r}}_k = \mathbf{f}(t, \mathbf{r}_k, \dot{\mathbf{r}}_k)$$

with initial conditions

$$\mathbf{r}_k(t_k) \doteq \mathbf{r}_{k0} \qquad \text{and} \qquad \dot{\mathbf{r}}_k(t_k) \doteq \dot{\mathbf{r}}_{k0}$$

where the initial values are defined as

$$\mathbf{r}_{k0}^{(i)} = \begin{cases} \mathbf{r}_0^{(i)} & ; \ k = 0 \\ \mathbf{r}_{k-1}^{(i)}(t_k) & ; \ k > 0 \end{cases}$$

Numerical Integration (3)

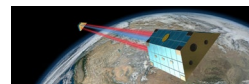The **collocation method** approximates the solution in the interval I_k by:

$$\mathbf{r}_k(t) \doteq \sum_{l=0}^{q} \frac{1}{l!} (t - t_k)^l \, \mathbf{r}_{k0}^{(l)}$$
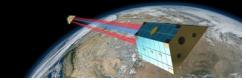
The coefficients $\mathbf{r}_{k0}^{(l)}$, $l = 0, ..., q$ are obtained by requesting that the numerical solution assumes the initial values and solves the differential equation system at $q - 1$ different epochs t_{k_j}, $j = 1, ..., q - 1$. This leads to the conditions

$$\sum_{l=2}^{q} \frac{(t_{k_j} - t_k)^{l-2}}{(l-2)!} \mathbf{r}_{k0}^{(l)} = \mathbf{f}(t_{k_j}, \mathbf{r}_k(t_{k_j}), \dot{\mathbf{r}}_k(t_{k_j})) \,, \quad j = 1, ..., q - 1.$$

They are non-linear but can be solved efficiently by an iterative procedure.

(Beutler, 2005)
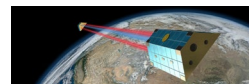
Partial Derivatives

The partial of the r -th observation w.r.t. orbit parameter P_i may be expressed as

$$\frac{\partial F_r(\boldsymbol{X})}{\partial P_i} = \left(\boldsymbol{\nabla} \left(F_r(\boldsymbol{X}) \right) \right)^T \cdot \frac{\partial \boldsymbol{r}_0}{\partial P_i}(t)$$

with the gradient given by

$$\left(\boldsymbol{\nabla} \left(F_r(\boldsymbol{X}) \right) \right)^T = \left(\frac{\partial F_r(\boldsymbol{X})}{\partial r_{0,1}} \quad \frac{\partial F_r(\boldsymbol{X})}{\partial r_{0,2}} \quad \frac{\partial F_r(\boldsymbol{X})}{\partial r_{0,3}} \right)$$

if the observations only depend on the geocentric position vector and are referring to only one epoch. The gradient only depends on the type of observations used, whereas the second term is independent of the observation type and related to the **variational equations**. This separates the observation-specific (**geometric**) part from the **dynamic** part.

Variational Equations

For each orbit parameter P_i the corresponding **variational equation** reads as

$$\ddot{\boldsymbol{z}}_{P_i} = \boldsymbol{A}_0 \cdot \boldsymbol{z}_{P_i} + \boldsymbol{A}_1 \cdot \dot{\boldsymbol{z}}_{P_i} + \frac{\partial \boldsymbol{f}_1}{\partial P_i}$$

with $\boldsymbol{z}_{P_i}(t) \doteq \dfrac{\partial \boldsymbol{r}_0}{\partial P_i}(t)$ and the 3 x 3 matrices defined by
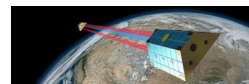
$$A_{0[i;k]} \doteq \frac{\partial f_i}{\partial r_{0,k}} \qquad \text{and} \qquad A_{1[i;k]} \doteq \frac{\partial f_i}{\partial \dot{r}_{0,k}}$$

f_i i-th component of the total acceleration $\boldsymbol{f}$

$r_{0,k}$ k-th component of the geocentric position $\boldsymbol{r}_0$
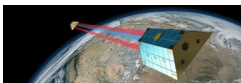
For each orbit parameter P_i the **variational equation** is a linear differential equation system of second order in time. Their solutions are all needed for orbit determination.
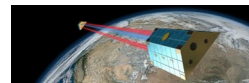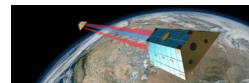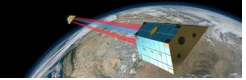
(Jäggi, 2007)

AIUB

$\boldsymbol{u}^b$
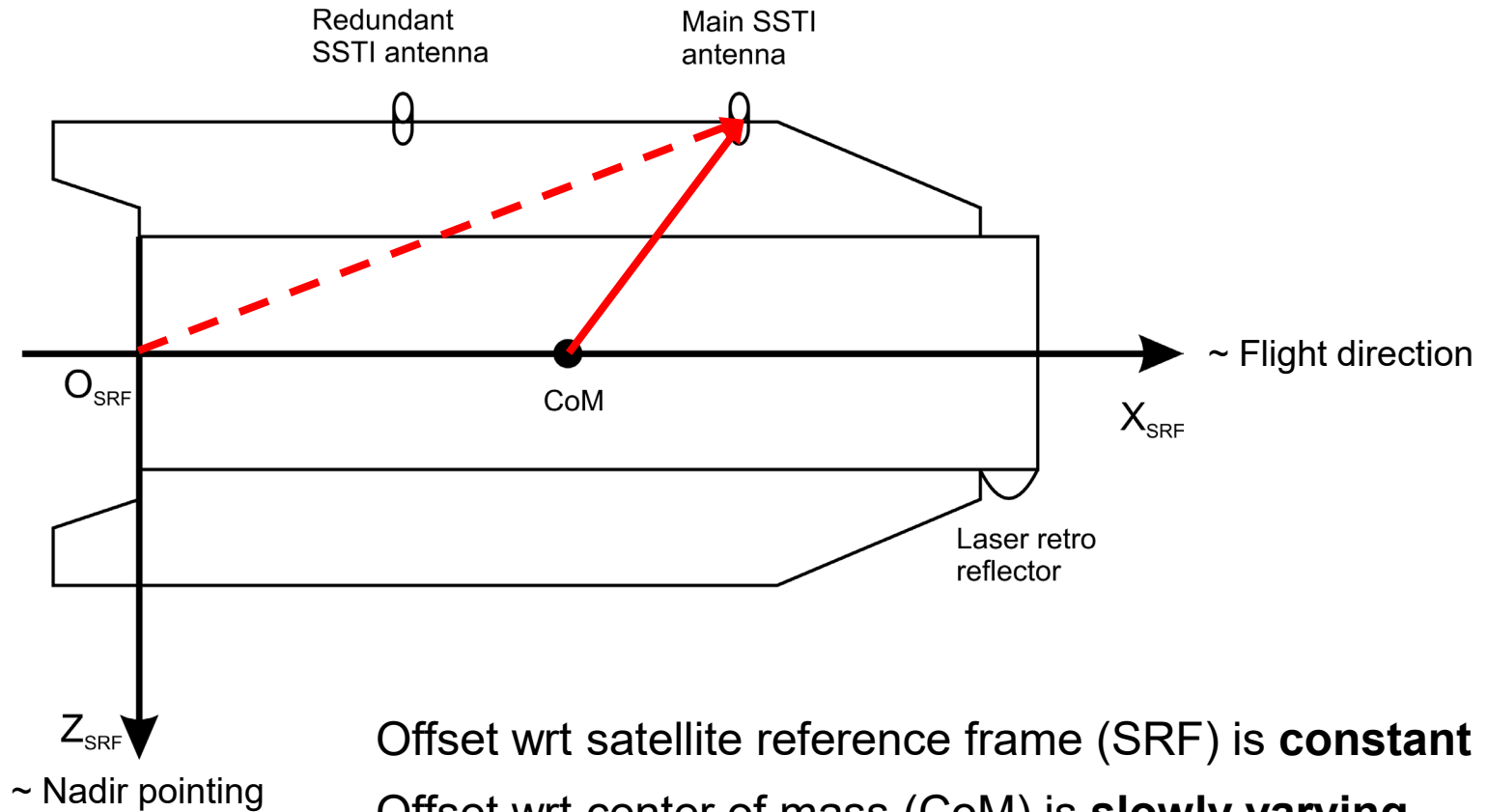UNIVERSITÄT
BERN

GPS-based LEO POD

LEO Sensor Offsets

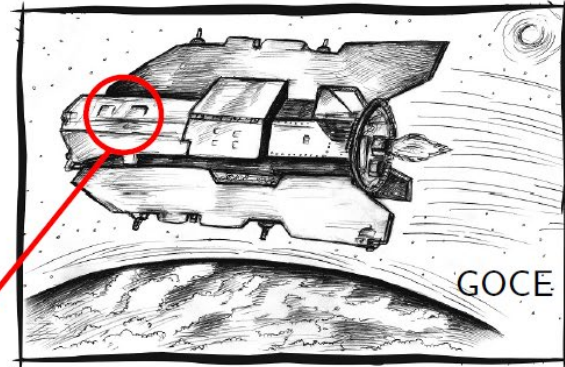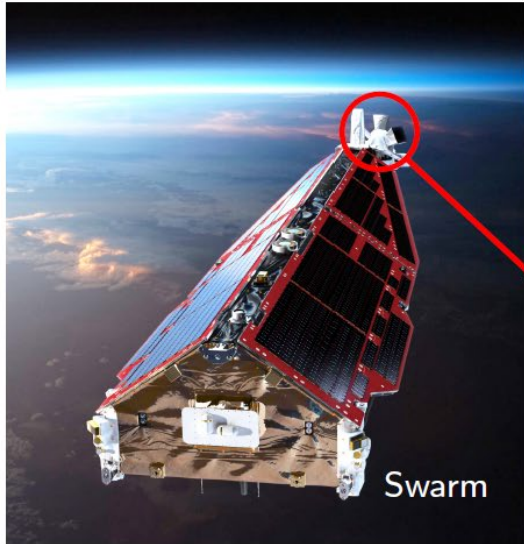**Phase center offsets** $\delta \boldsymbol{r}_{leo,ant}$:

- are needed in the inertial or Earth-fixed frame and have to be transformed from the satellite frame using **attitude data** from the star-trackers

- consist of a frequency-independent **instrument offset**, e.g., defined by the center of the instrument's mounting plane (CMP) in the satellite frame

- consist of frequency-dependent **phase center offsets** (PCOs), e.g., defined wrt the center of the instrument's mounting plane in the antenna frame (ARF)

- consist of frequency-dependent **phase center variations** (PCVs) varying with the direction of the incoming signal, e.g., defined wrt the PCOs in the antenna frame
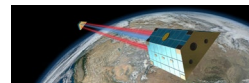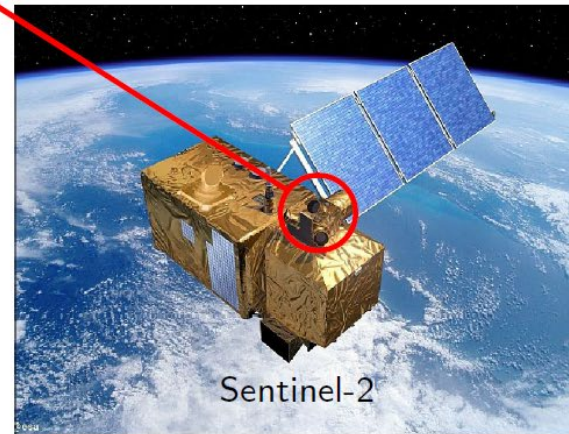
Example: GOCE Sensor Offsets (1)

Offset wrt satellite reference frame (SRF) is **constant**

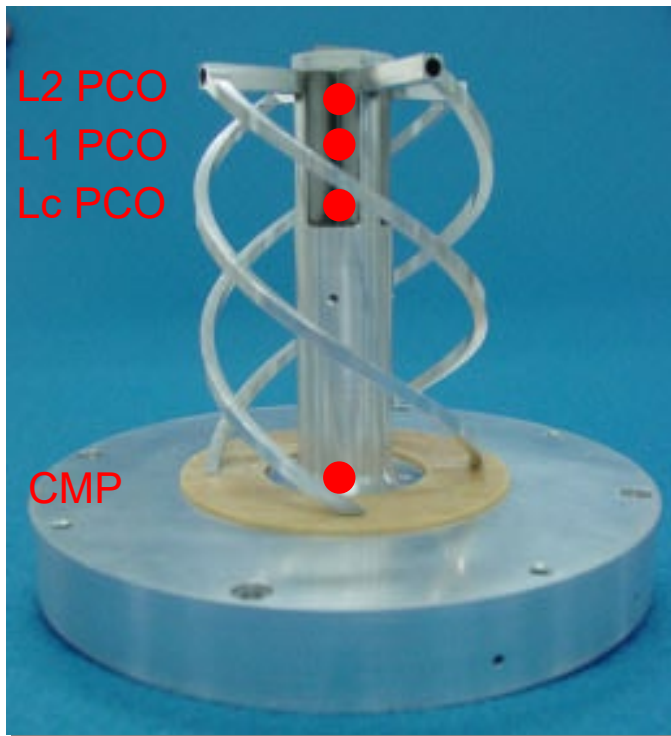Offset wrt center of mass (CoM) is **slowly varying**
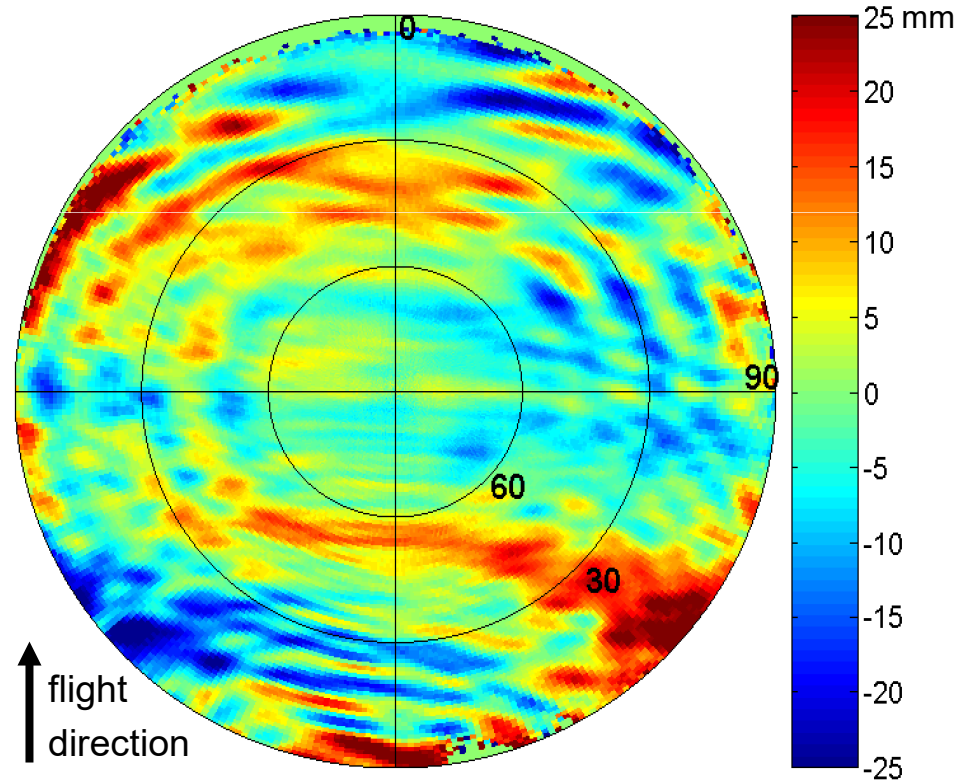
Example: GOCE Sensor Offsets (2)

Spaceborne GPS Antennas: GOCE

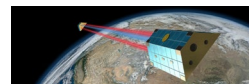## L1, L2, Lc phase center offsets

Measured from ground calibration
in anechoic chamber

Lc phase center variations

flight
direction

Empirically derived during orbit determination
according to Jäggi et al. (2009)

Spaceborne GPS Antennas: Swarm

Swarm GPS antenna

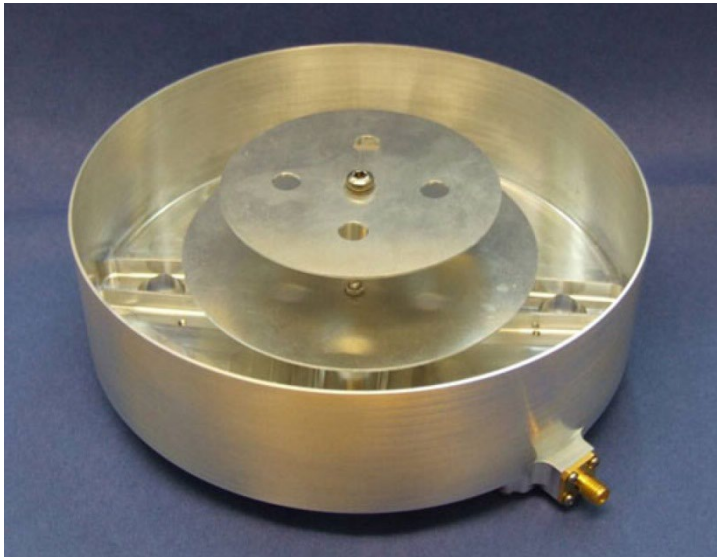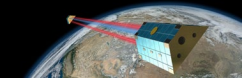Multipath shall be minimzed by chokering

Lc phase center variations

flight direction
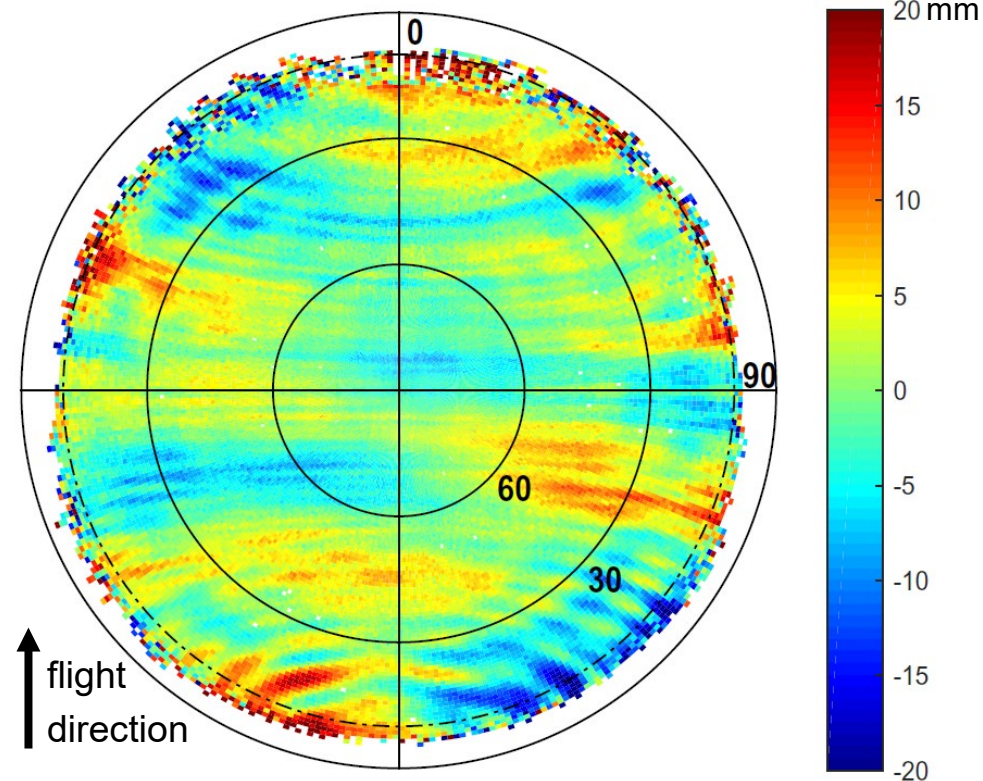
Empirically derived during orbit determination according to Jäggi et al. (2016)

Spaceborne GPS Antennas: GRACE

flight direction

GRACE-A
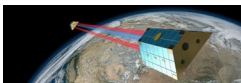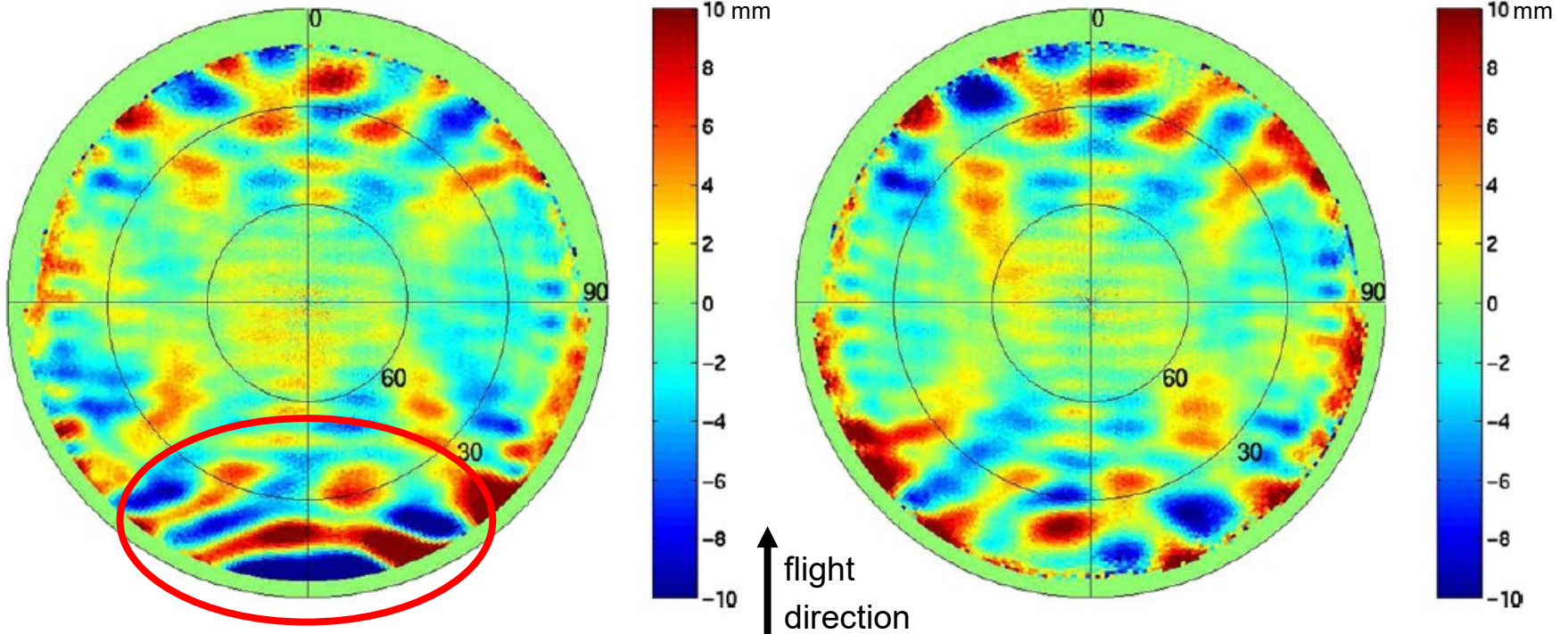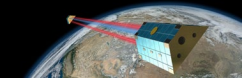(occultation antenna switched on)

GRACE-B

(Jäggi et al., 2009)
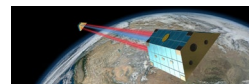
Visualization of Orbit Solutions
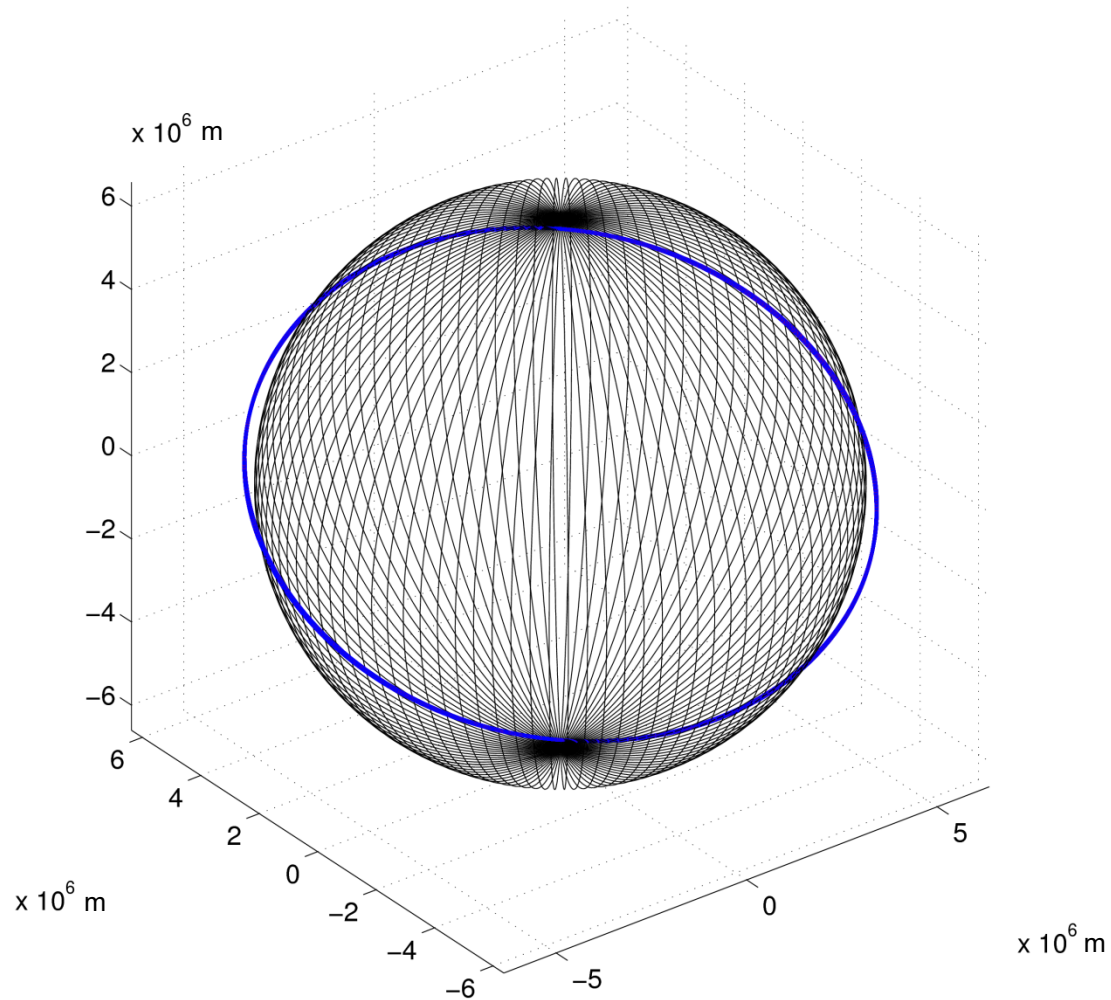
It is more instructive to look at differences between orbits in well suited coordinate systems …

AIUB

UNIVERSITÄT BERN
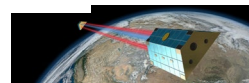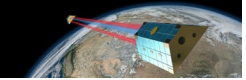
Co-Rotating Orbital Frames
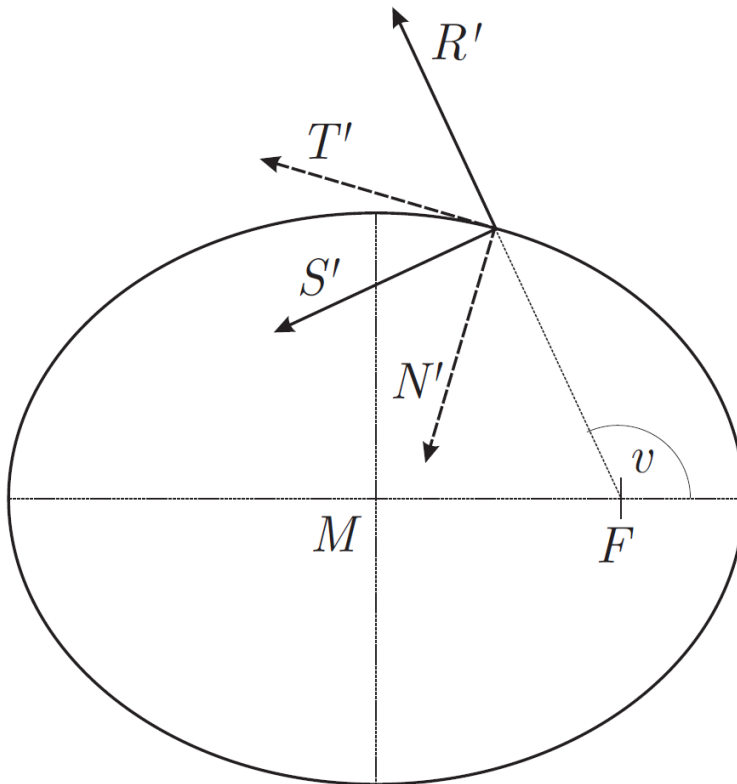
R, S, C unit vectors are pointing:

-   into the radial direction

-   normal to **R** in the orbital plane

-   normal to the orbital plane (cross-track)

T, N, C unit vectors are pointing:

-   into the tangential (along-track) direction

-   normal to **T** in the orbital plane

-   normal to the orbital plane (cross-track)

Small eccentricities: **S~T** (velocity direction)
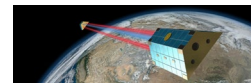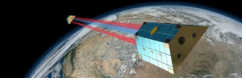
Orbit Differences KIN-RD (Sentinel-3A)

Differences at epochs of kin. positions
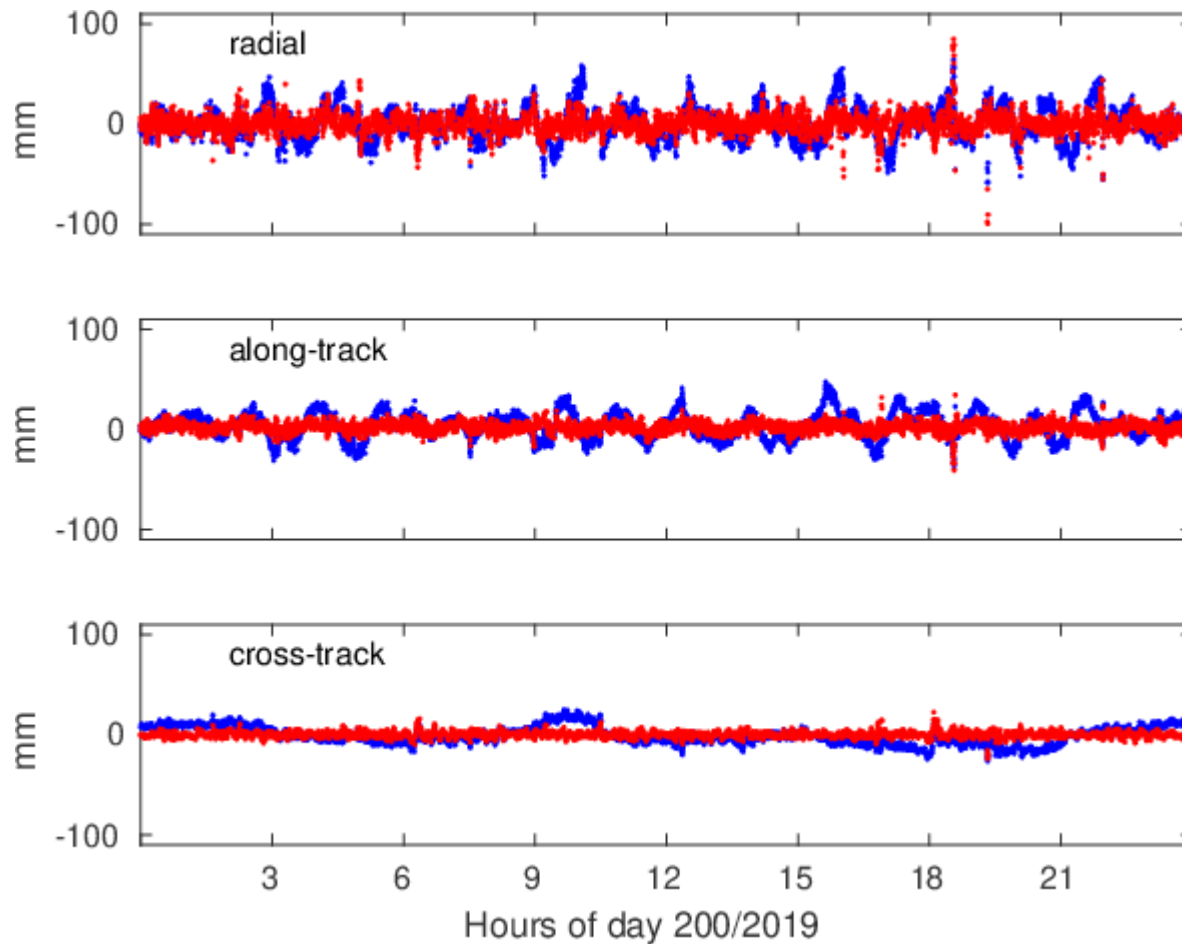
Comparison of ambiguity-float solutions and ambiguity-fixed solutions.

Orbit Differences KIN-RD (COSMIC-2)

Differences at epochs of kin. positions, FM-1, POD-1
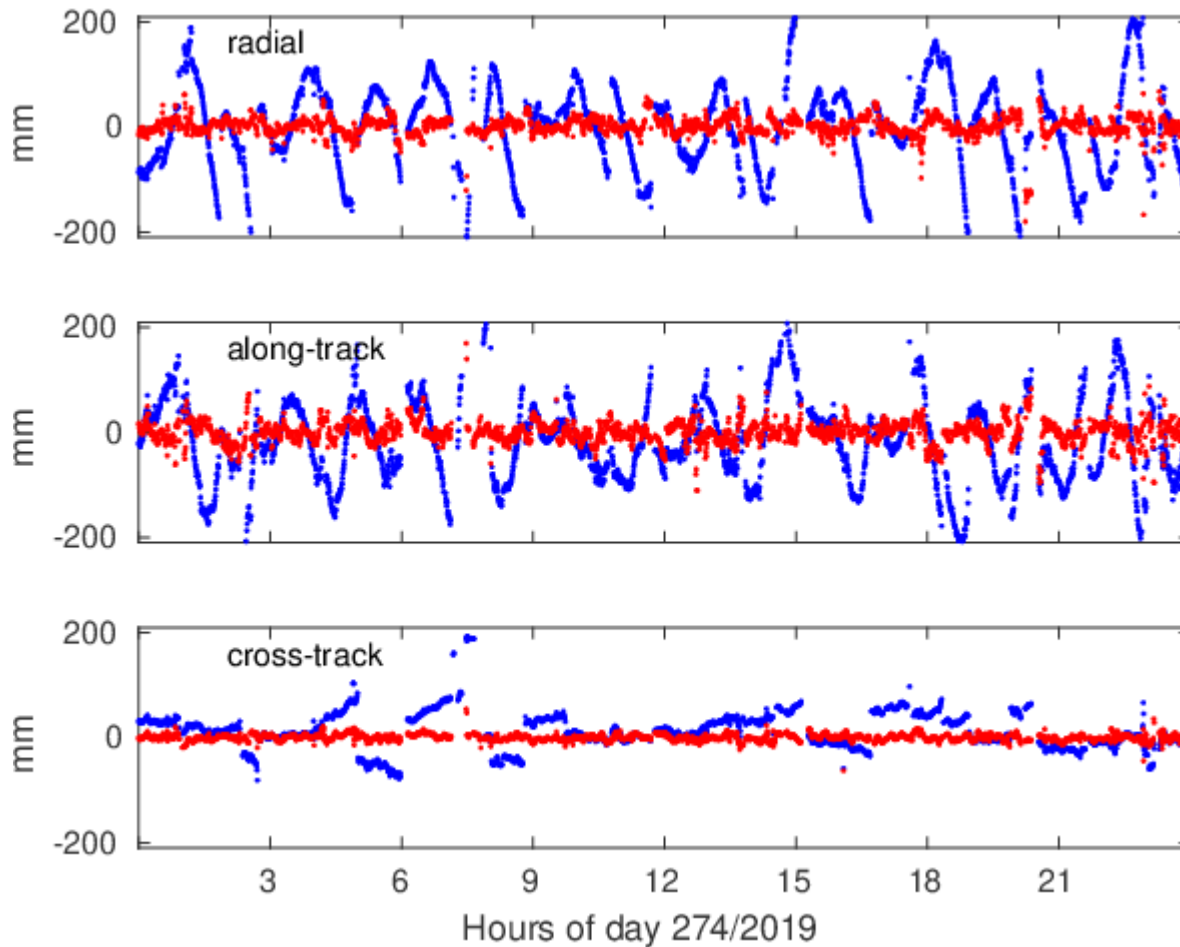
Comparison of ambiguity-float solutions and ambiguity-fixed solutions. (Jäggi et al. 2021)
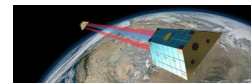
Orbit Differences KIN-RD (GOCE)
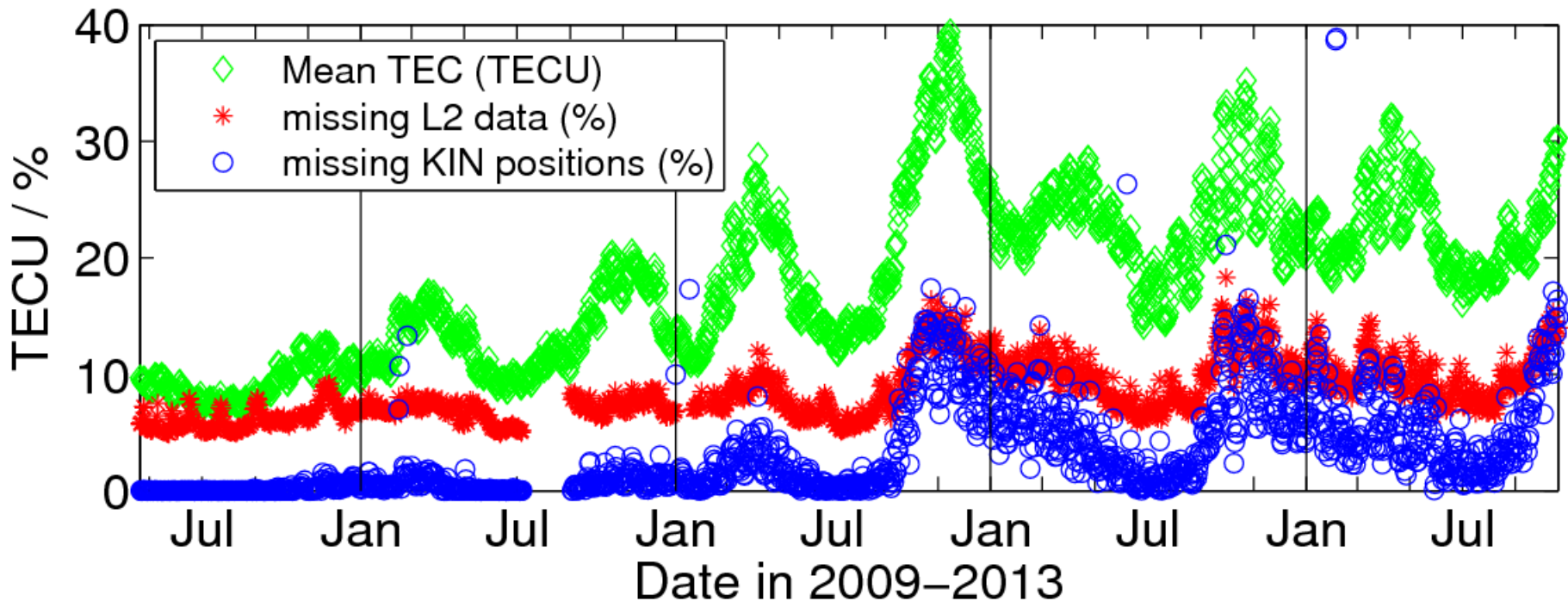
The result illustrates the **consistency** between both orbit-types for the GOCE Precise Science Orbit (PSO) product. The level of the differences is usually given by the quality of the kinematic positions. The differences are highly correlated with the **ionosphere activity** and with **data losses on L2**.

(Bock et al., 2014)

RMS of Carrier Phase Residuals (Sentinel-1)
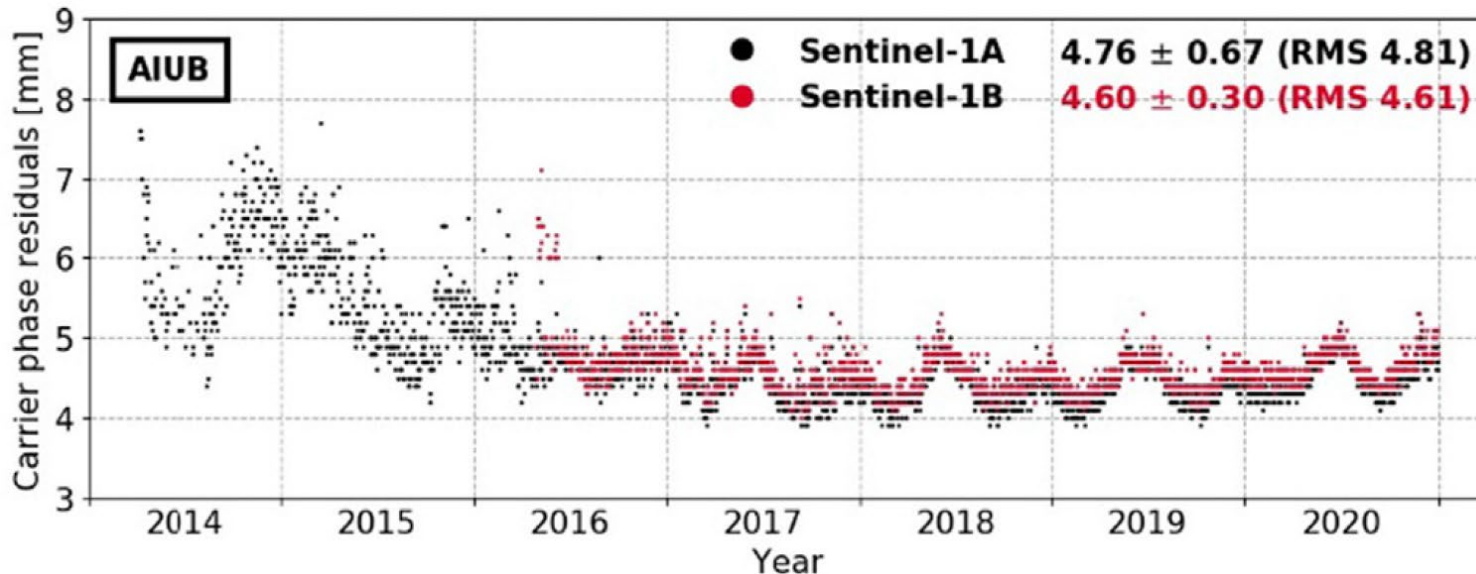
The plot illustrates the **quality** of the orbit fit. The level is given by the adopted parametrization, depending on how dynamic the orbit parametrization is.

The variations reveal again the impact of the **ionosphere activity** and also further **modeling deficiencies.**

(Fernández et al., 2022)
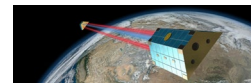
Consequences of Ionospheric Effects in Orbits

For GOCE systematic effects around the geomagnetic equator were observed in the ionosphere-free GPS phase residuals **=> affects kinematic positions**

Degradation of kinematic positions around the geomagnetic equator propagates into gravity field solutions.

mean residuals at Ionosphere-crossing: 2011, doys 245–365

x 10⁻³
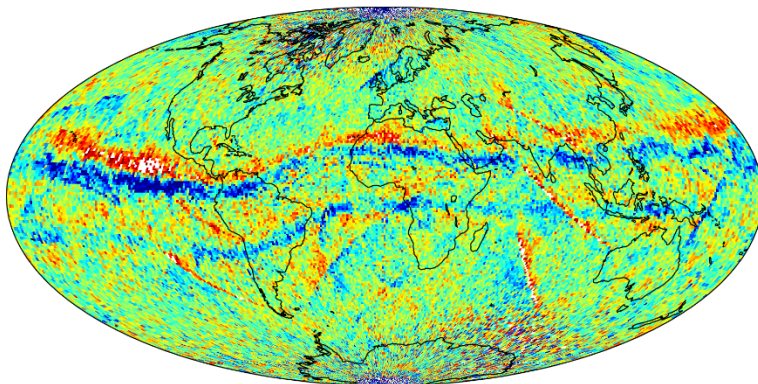
Phase observation residuals
(- 2 mm … +2 mm) mapped
to the ionosphere piercing
point
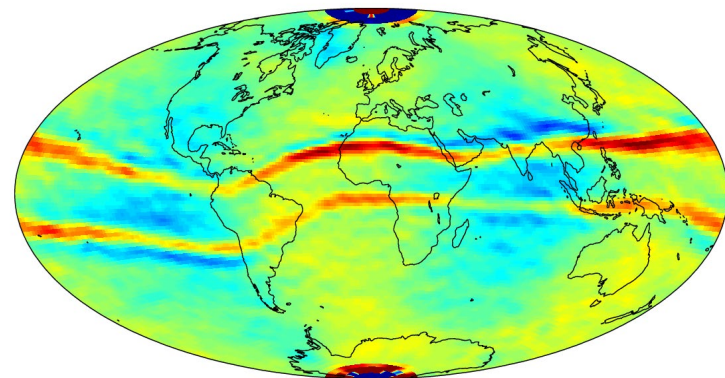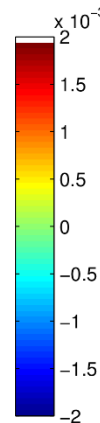
Geoid height differences
(−5 cm … 5 cm);
R4 period

(Jäggi et al., 2015)

AIUB

u^b

UNIVERSITÄT
BERN
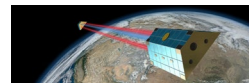
Systematic Errors in GPS Data (1)

Original GPS Data
(Swarm)

Original GPS Data
(GRACE)

min/max/wrms [m]: −0.042/0.052/0.010

[m]

−0.05 −0.04 −0.03 −0.02 −0.01 0.00 0.01 0.02 0.03 0.04 0.05

min/max/wrms: −2.33 / 3.28 / 0.54

[cm]

-4   -2   0   2   4
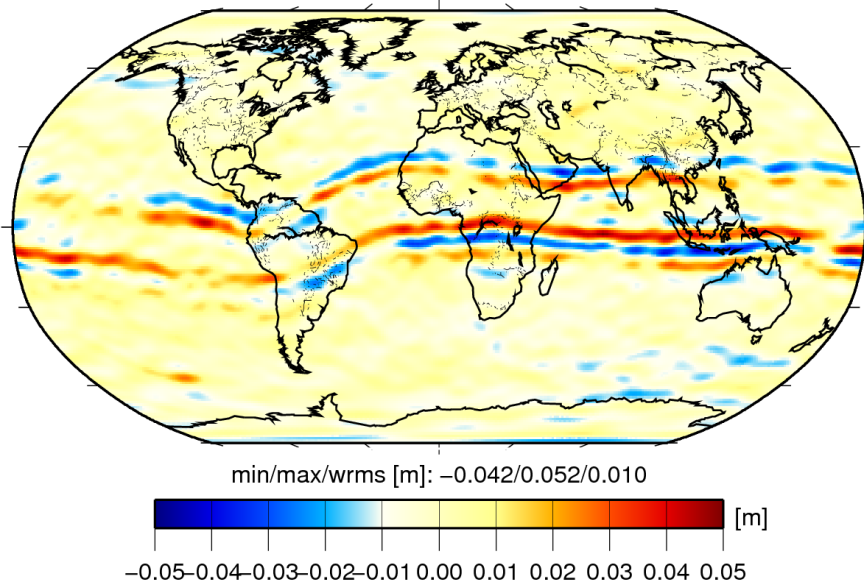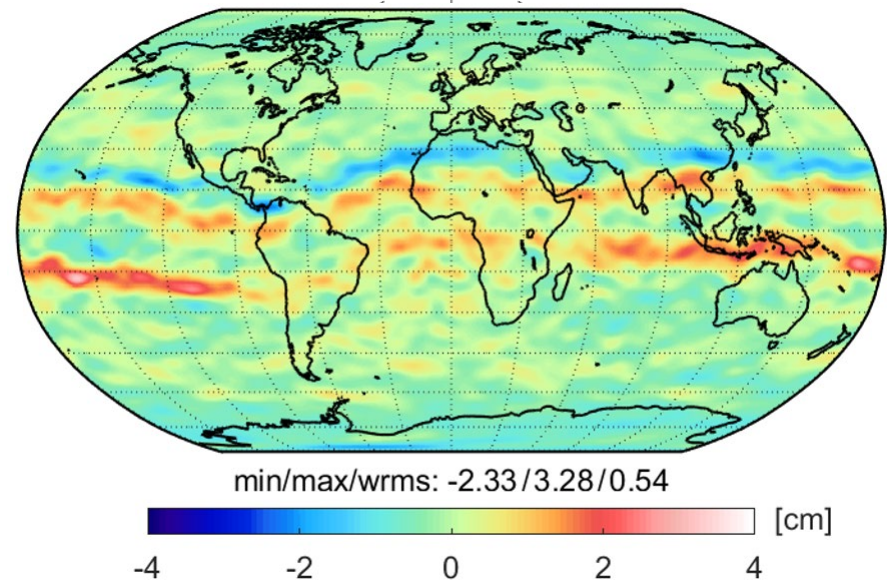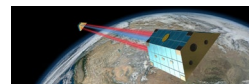
(Differences wrt GOCO05S, 400 km Gauss smoothing adopted)

Systematic signatures along the geomagnetic equator are **"not"** visible when using original L1B RINEX GPS data files from the GRACE mission.

(Jäggi et al., 2016)

AIUB u^b

UNIVERSITÄT
BERN

Systematic Errors in GPS Data (2)
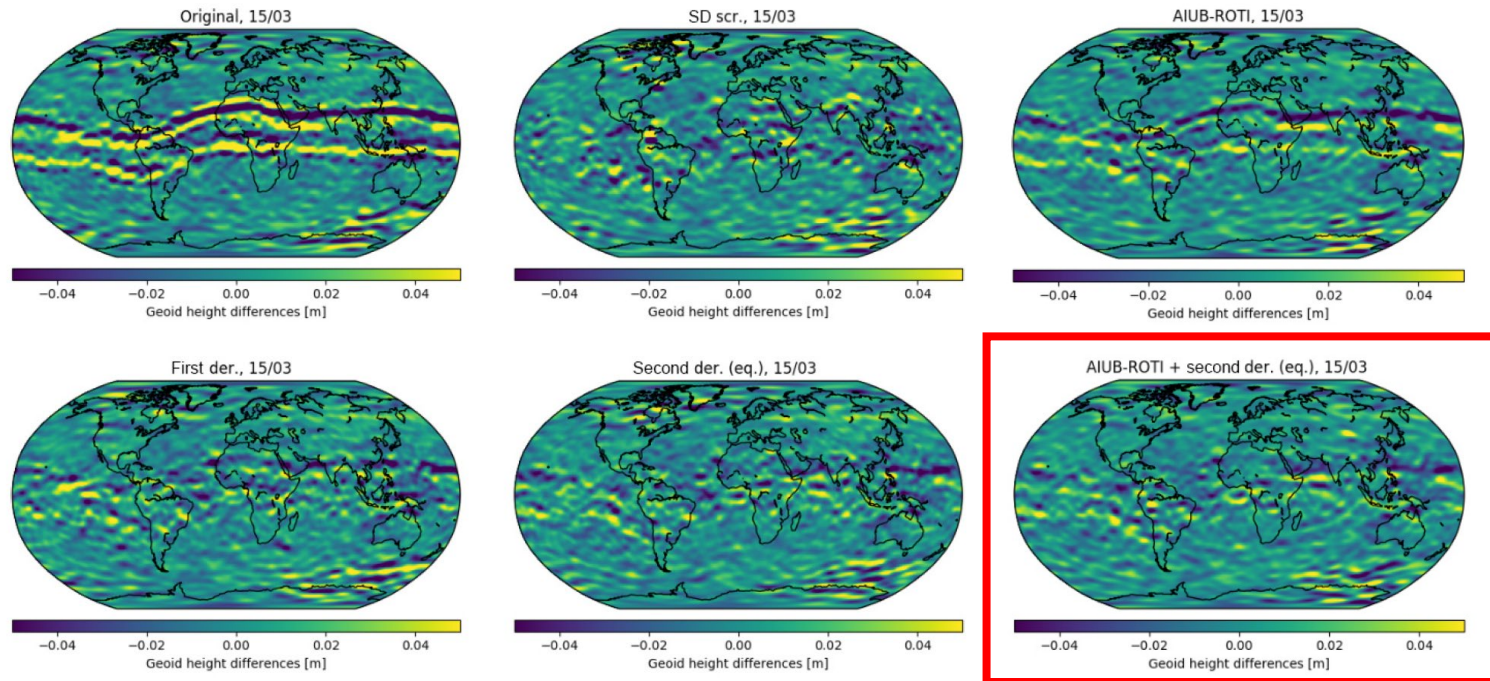
(Differences wrt JPL-GRACE-RL06, 400 km Gauss smoothing adopted)

Systematic signatures along the geomagnetic equator may be efficiently reduced when down-weighting the GPS data using derivatives of the geometry-free linear combination. ROTI-based down-weighting additionally reduces scintillation noise.

(Schreiter et al., 2019)

Systematic Errors in GPS Data (3)
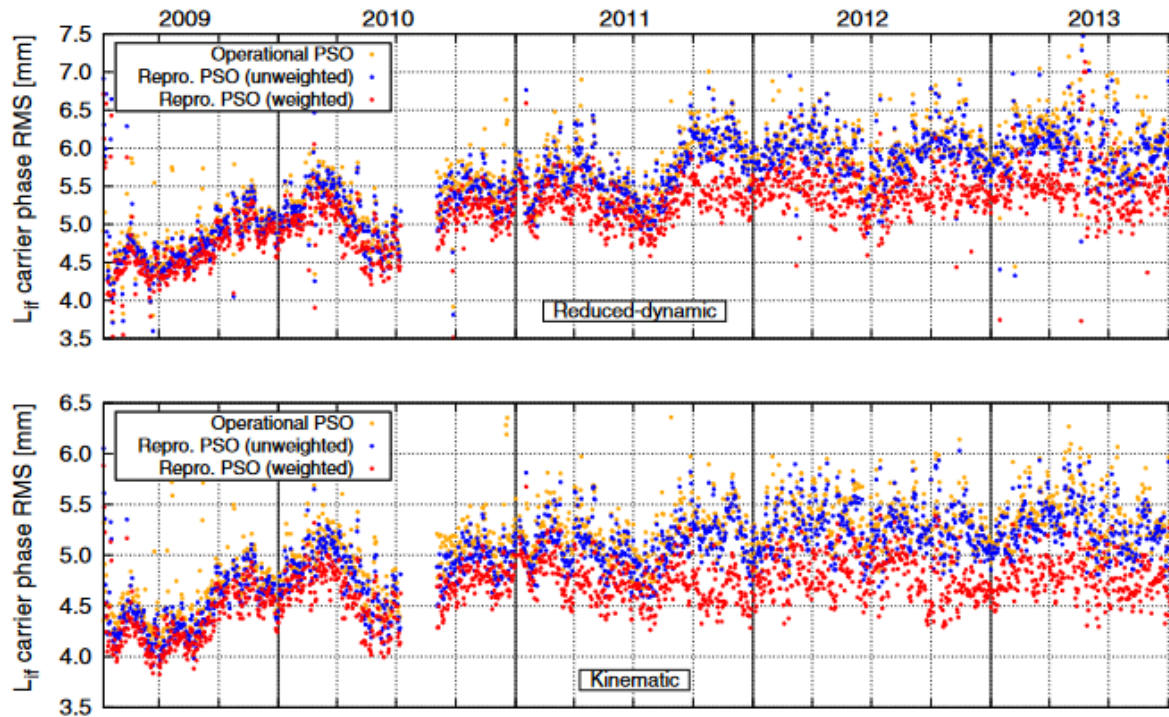
The plot illustrates the importance of adequate weighting strategies, as they were used for the reprocessing of the GOCE Precise Science Orbits, for the quality of the orbit fit when high ionosphere activity is present.

(Arnold et al., 2023)
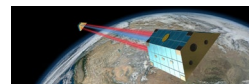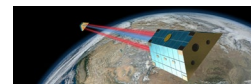
Systematic Errors in GPS Data (4)
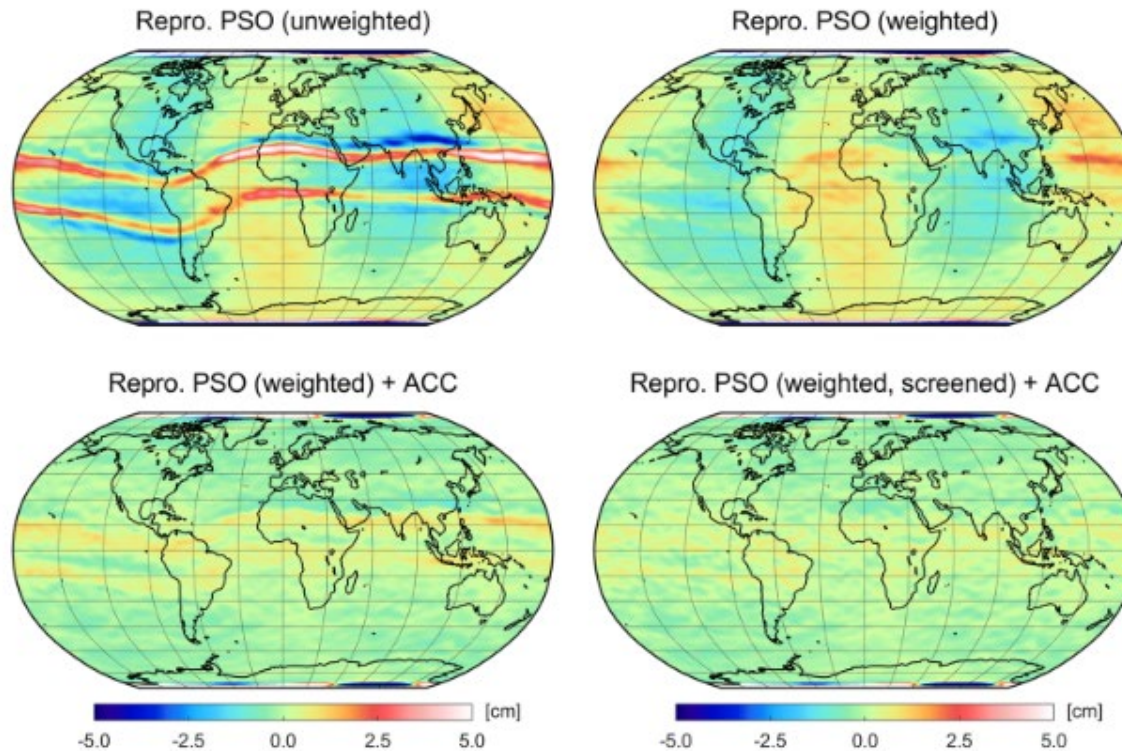
(Differences wrt ITSG-Grace2018, 300 km Gauss smoothing adopted)

Remarkable reduction of ionosphere-induced artifacts along the geomagnetic equator when using the kinematic positions of the reprocessed GOCE Precise Science Orbits for gravity field recovery.
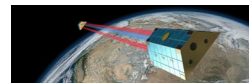
(Arnold et al., 2023)

Sensitivity to the Time-Variable Gravity Field Model (1)
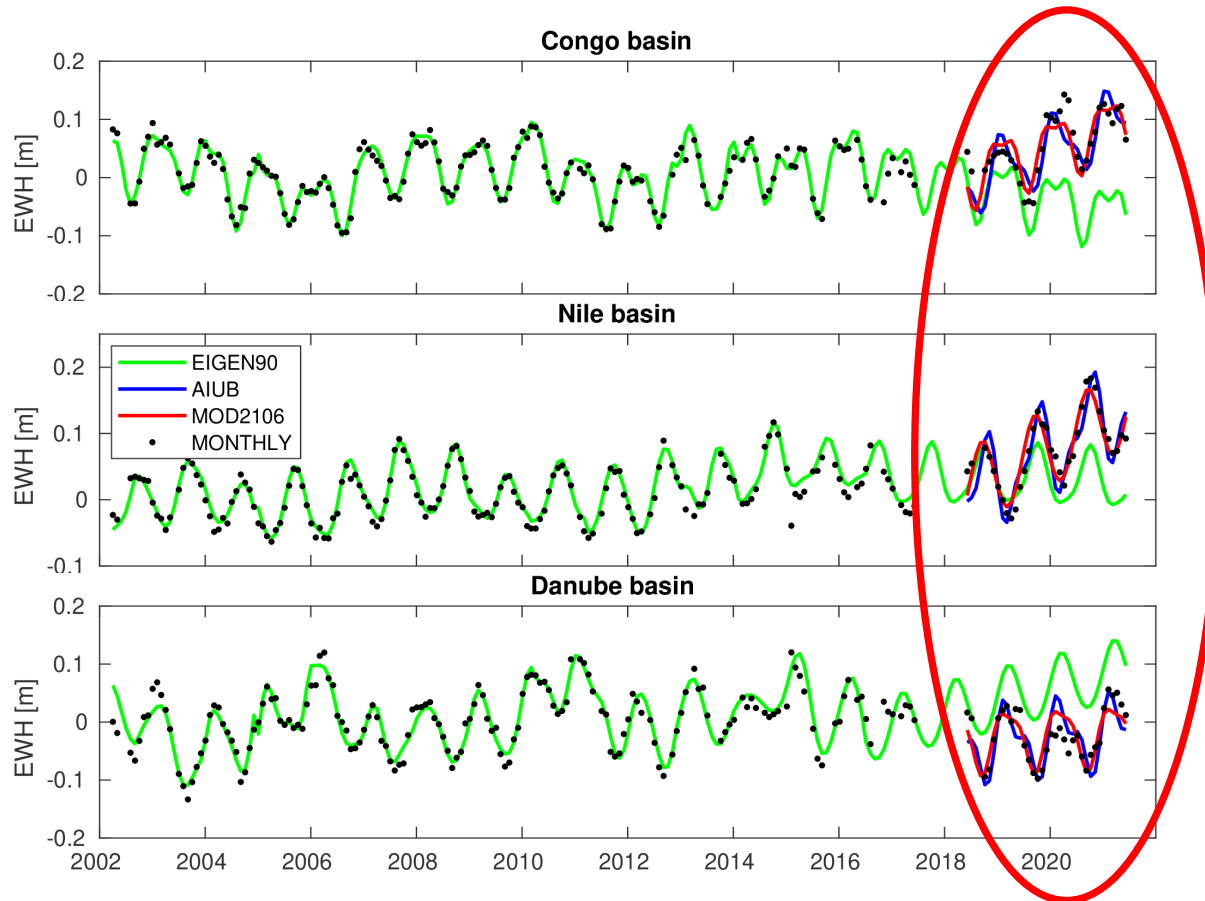
The predictions of the EIGEN-GRGS.RL04 model (containing no data after 2017) are rather poor as shown here for three river basins. The fitted signal model (FSM) to COST-G monthly solutions has clear advantages. (Peter et al., 2022)

Sensitivity to the Time-Variable Gravity Field Model (2)
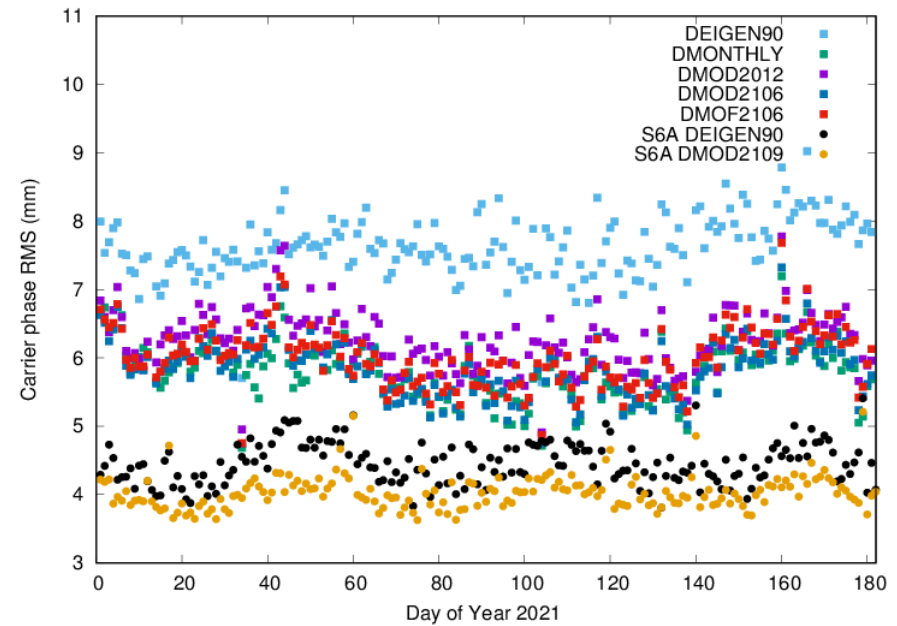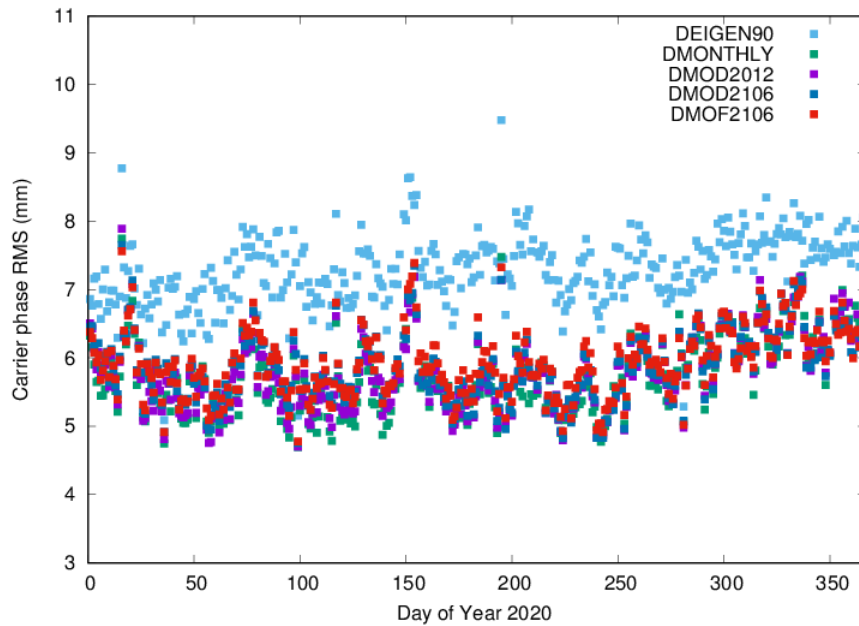
Monthly COST-G GRACE-FO gravity fields (▪) outperform GRACE-based static fields (▪) with co-estimated time-variations for Sentinel-3B (left and right plot).

COST-G fitted signal models (FSM) perform comparably good (▪ ▪ ▪, left plot), which also holds for Sentinel-6A (●, right plot). In particular the COST-G FSM show also good prediction capabilities (▪, right plot).

(Peter et al., 2022)

Orbit Validation

Orbit Comparisons (Spire FM099)

Daily RMS values AIUB red.–dyn. vs. Spire (FM099), obs. pos.

AIUB – Spire

Radial (17.8 cm)
Along–track (16.6 cm)
Cross–track (11.4 cm)
3D (27.2 cm)

Daily RMS values AIUB red.–dyn. vs. PosiTim (FM099), obs. pos.

AIUB – PosiTim

Radial (4.7 cm)
Along–track (5.2 cm)
Cross–track (3.7 cm)
3D (7.9 cm)
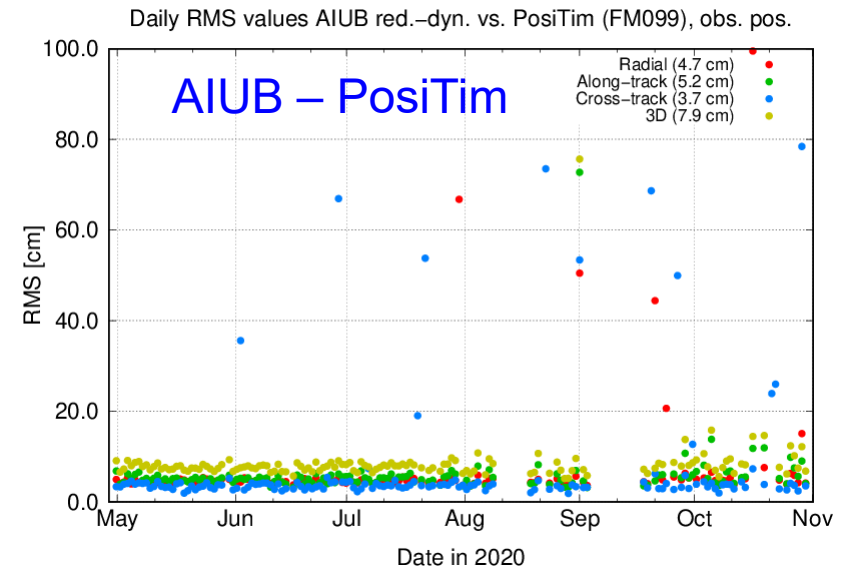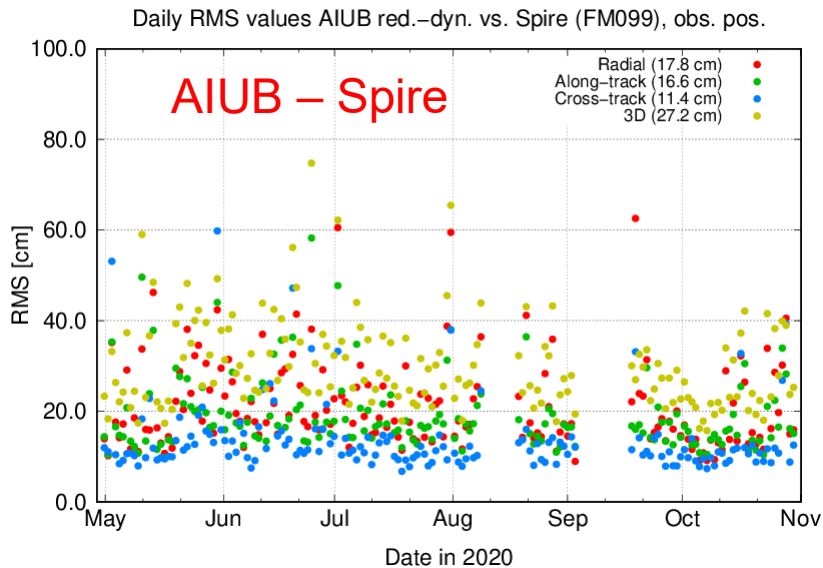
Orbit comparisons between solutions computed **with different software packages** are helpful, especially if no external orbit validations are possible.

The plots show for the example of one Spire satellite that orbit differences AIUB – PosiTim are significantly smaller than the orbit differences AIUB – Spire.

(Jäggi et al., 2022)
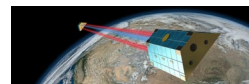
GRACE Orbit Validation with K-Band

ZD solution
< 1cm

DD solution
(ambiguity-fixed)
< 1mm
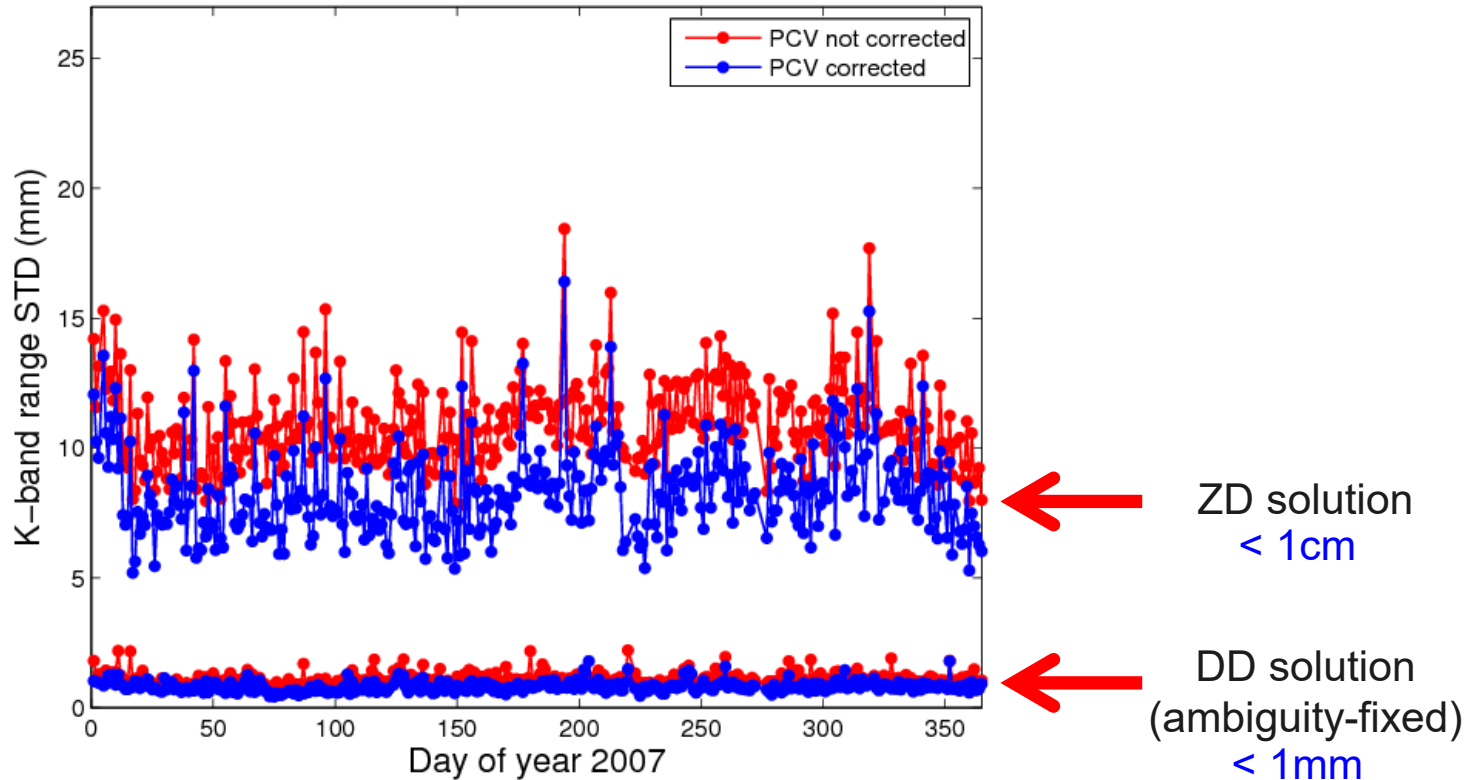
The ultra-precise and continuously available K-Band data allow it to validate the **inter-satellite distances** between the GRACE satellites. Thanks to this validation, e.g., PCV maps were recognized to be crucial for high-quality POD.

(Jäggi et al., 2009)

Orbit Validation with SLR (GOCE)

SLR Residuals for GOCE (RD PSO orbit)

Reduced-dynamic

SLR statistics:

Mean ± RMS (cm)

Year	red.-dynamic	kinematic
2009	0.24 ± 1.73	0.29 ± 1.91
2010	-0.10 ± 1.56	-0.12 ± 1.84
2011	0.20 ± 1.53	0.12 ± 2.36
2012	0.10 ± 1.94	-0.05 ± 2.78
2013	0.63 ± 2.62	0.45 ± 3.17
2009–2013	0.18 ± 1.84	0.10 ± 2.42

Kinematic

(Bock et al., 2014)

AIUB

UNIVERSITÄT BERN

Impact of Undifferenced Ambiguity Resolution (1)

SLR Validation of Sentinel-3A
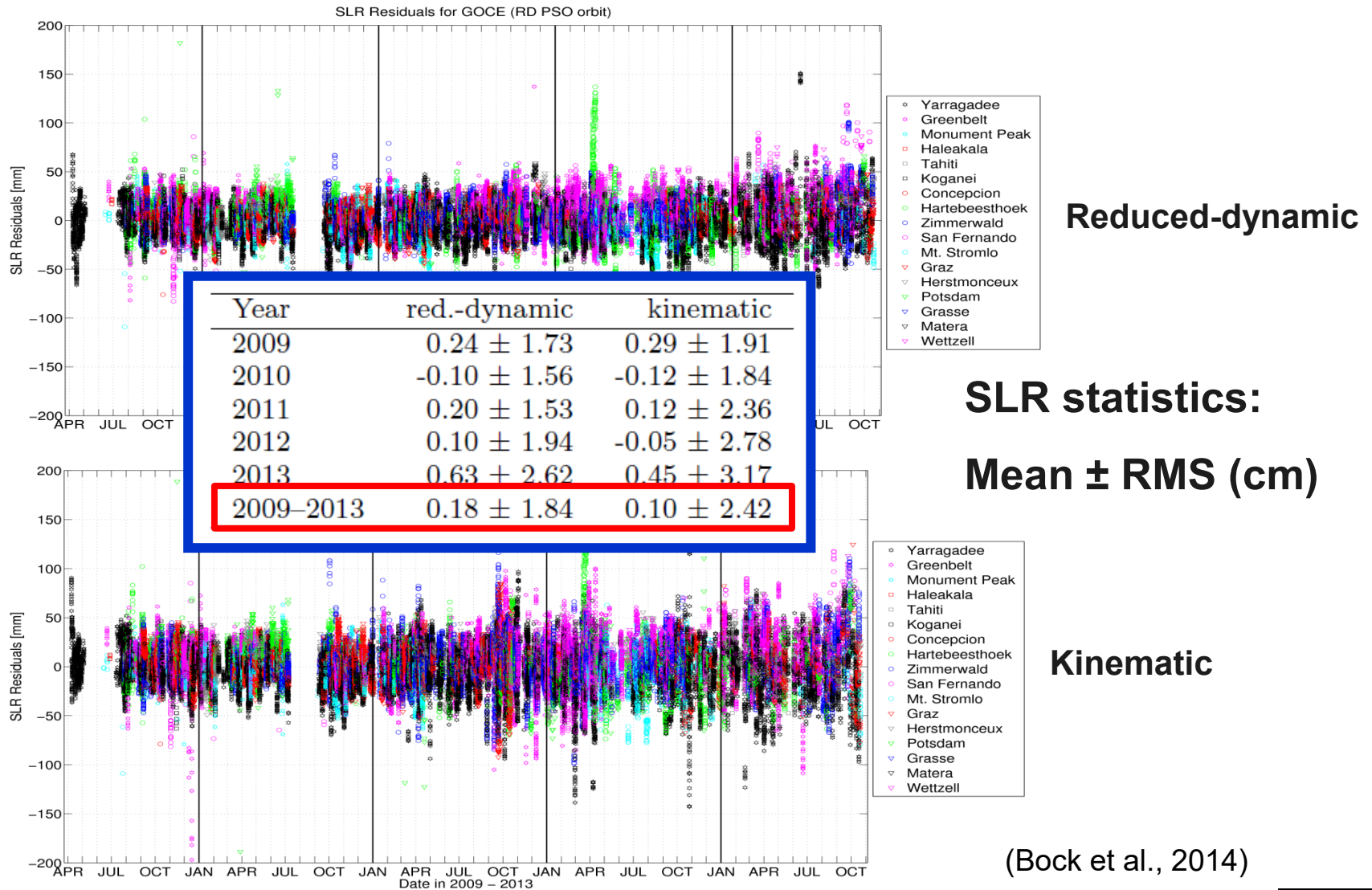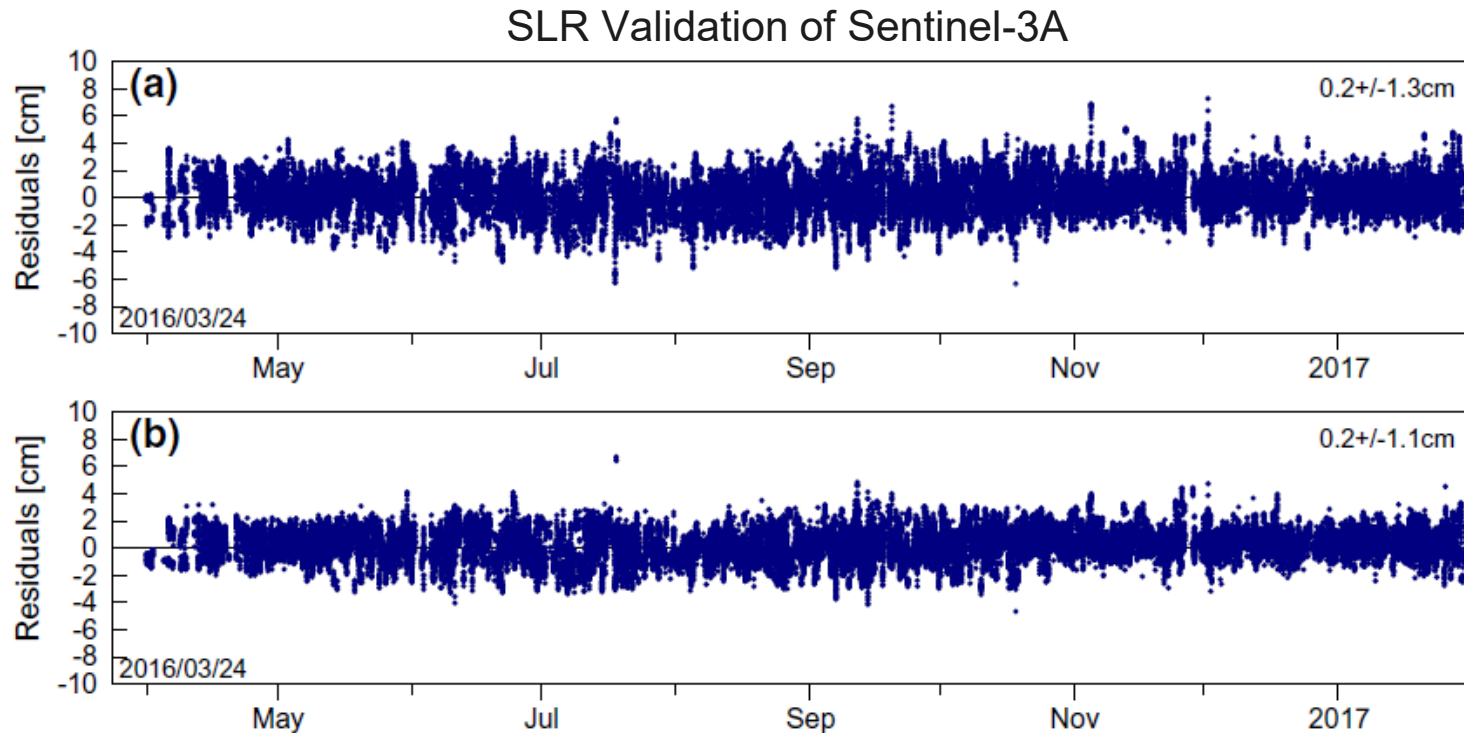
Single-receiver ambiguity fixing may be enabled by using phase bias products and corresponding clock products provided by the IGS analysis centers without the need to form any baselines. It allows to identify lateral offsets in the GPS antenna or center-of-mass location and to significantly stabilize the LEO trajectories.

(Montenbruck et al., 2018)

AIUB

u^b

UNIVERSITÄT
BERN
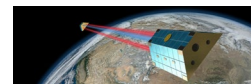
Impact of Undifferenced Ambiguity Resolution (2)
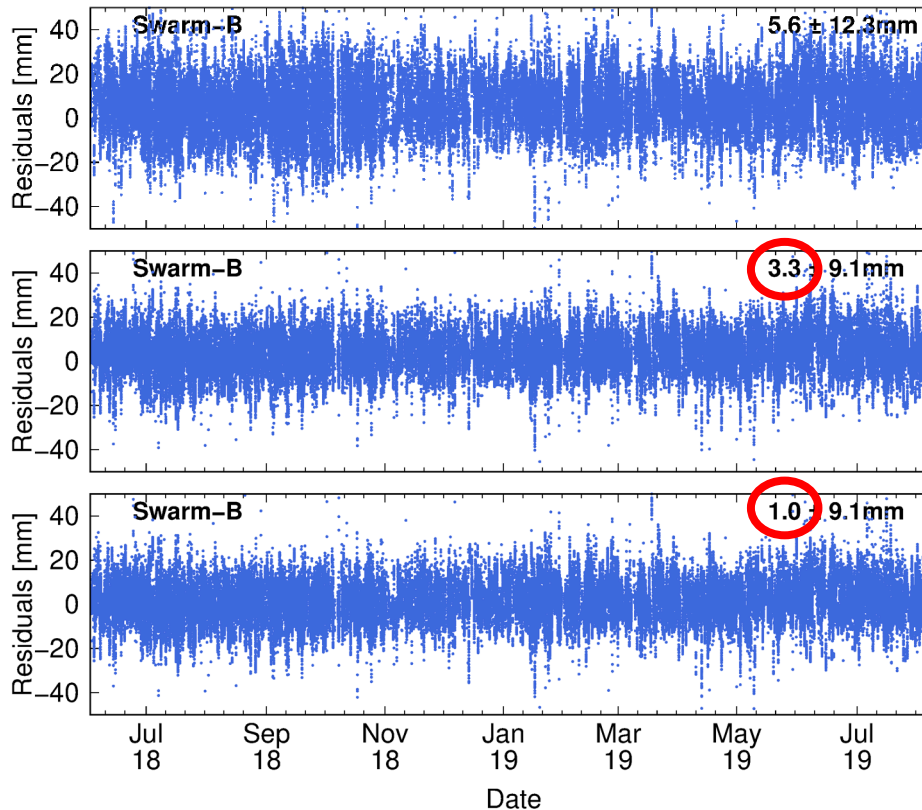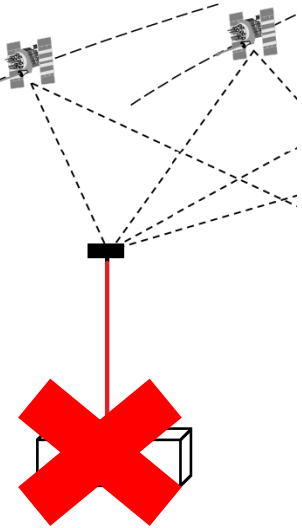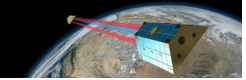
Ambiguity-float, no non-grav. modeling

Ambiguity-fixed, no non-grav. modeling

Ambiguity-fixed, with non-grav. modeling

LEO POD significantly profits from single-receiver ambiguity fixing techniques and high-quality signal-specific phase bias products, e.g., by Schaer et al. (2021).

(Arnold et al., 2019; Mao et al., 2021)

Impact of Undifferenced Ambiguity Resolution (3)

Kinematic, ambiguity-float

Kinematic, ambiguity-fixed
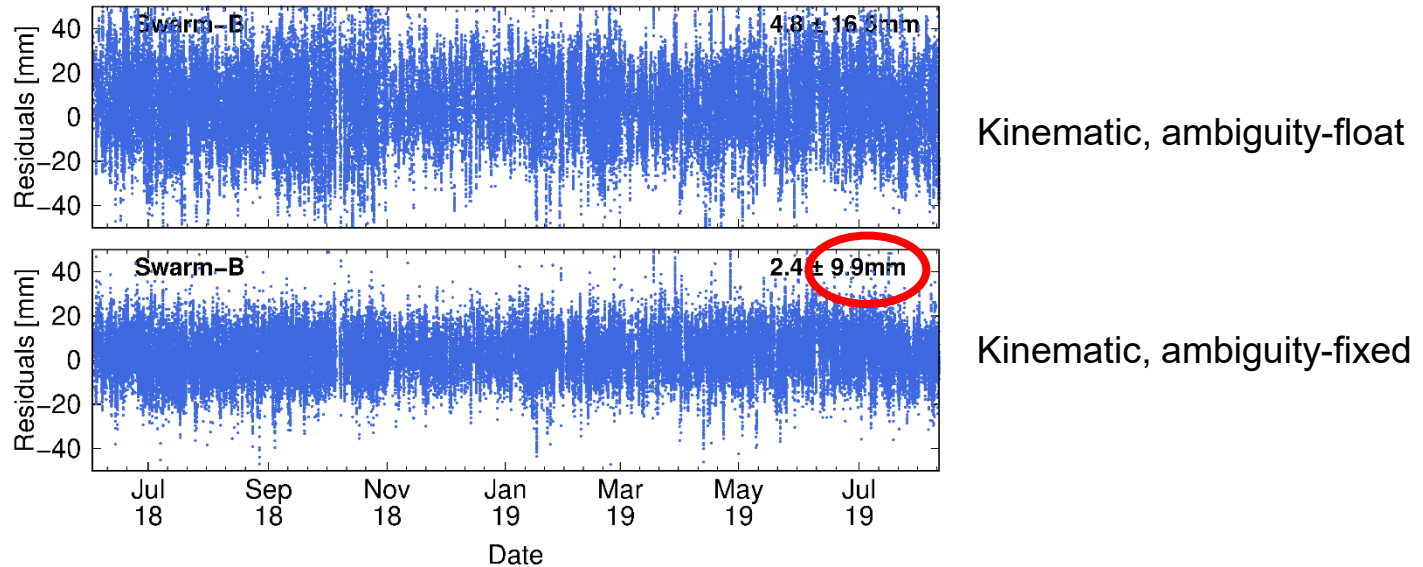
The SLR STD of ambiguity-fixed kinematic orbits (9.9mm) is only marginally worse than for the ambiguity-fixed dynamic orbits (9.1mm, see previous slide).

This nicely illustrates the limitation of SLR to "distinguish" between the orbits.

Comparisons to ambiguity-fixed kinematic orbits should be regularly performed to detect inconsistencies, e.g., related to wrong GPS antenna phase center offsets.
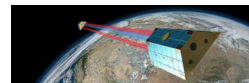
Orbit Validation – or SLR Network Validation?

Corrections from 1-year of dynamic, ambiguity-fixed Swarm-A/B/C, Sentintel-3A/B and GRACE-FO-C/D orbits.

compared to 1.5 ± 10.5 mm

Sentinel-3A   0.0 ± 7.8mm
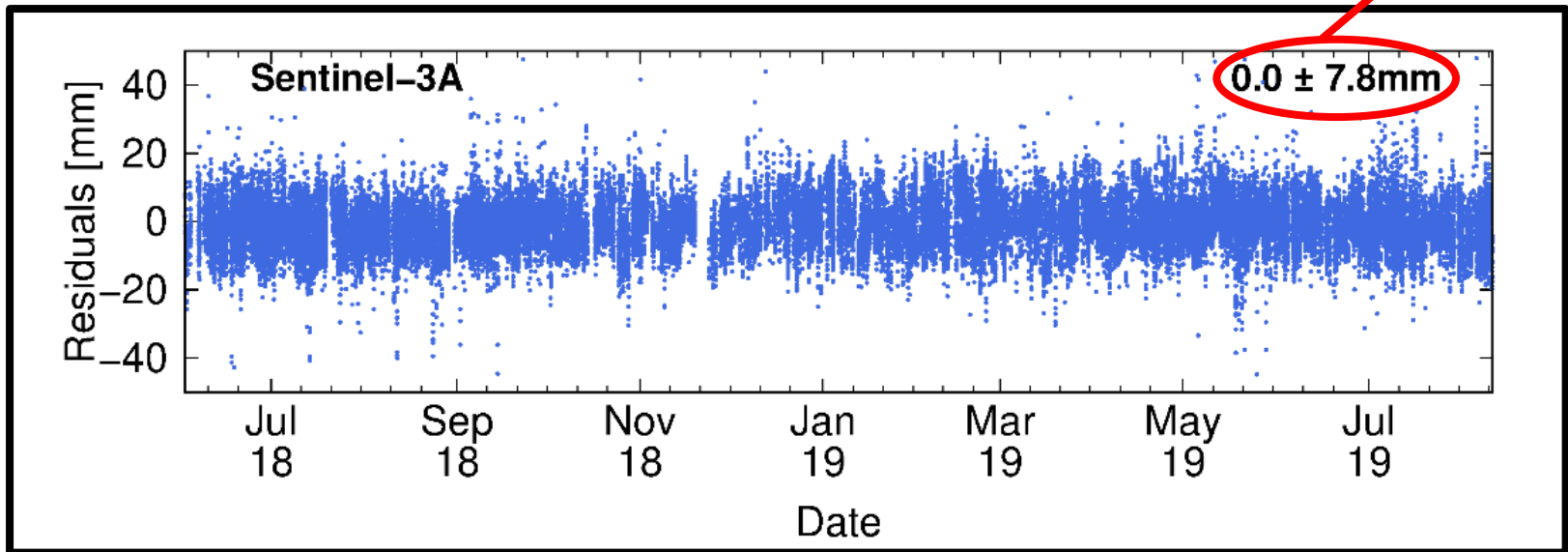
Graz	78393402	2.7 ± 0.2	3.2 ± 0.2	8.7 ± 0.7	11.9 ± 0.4
Herstmonceux	78403501	3.1 ± 0.3	1.5 ± 0.3	-4.1 ± 1.0	-2.5 ± 0.6
Potsdam	78418701	0.9 ± 0.3	3.7 ± 0.3	17.1 ± 0.9	-0.6 ± 0.6
Matera	79417701	1.7 ± 0.4	4.8 ± 0.4	4.2 ± 2.0	-5.3 ± 1.0

Some larger corrections ask for further investigations, e.g. comparisons to LAGEOS-based coordinate solutions. Investigations are on-going …

(Arnold et al., 2019)
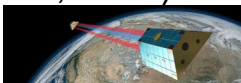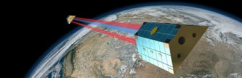
Multi-GNSS LEO POD

SLR Validation of Sentinel-6A

Station offsets adjusted
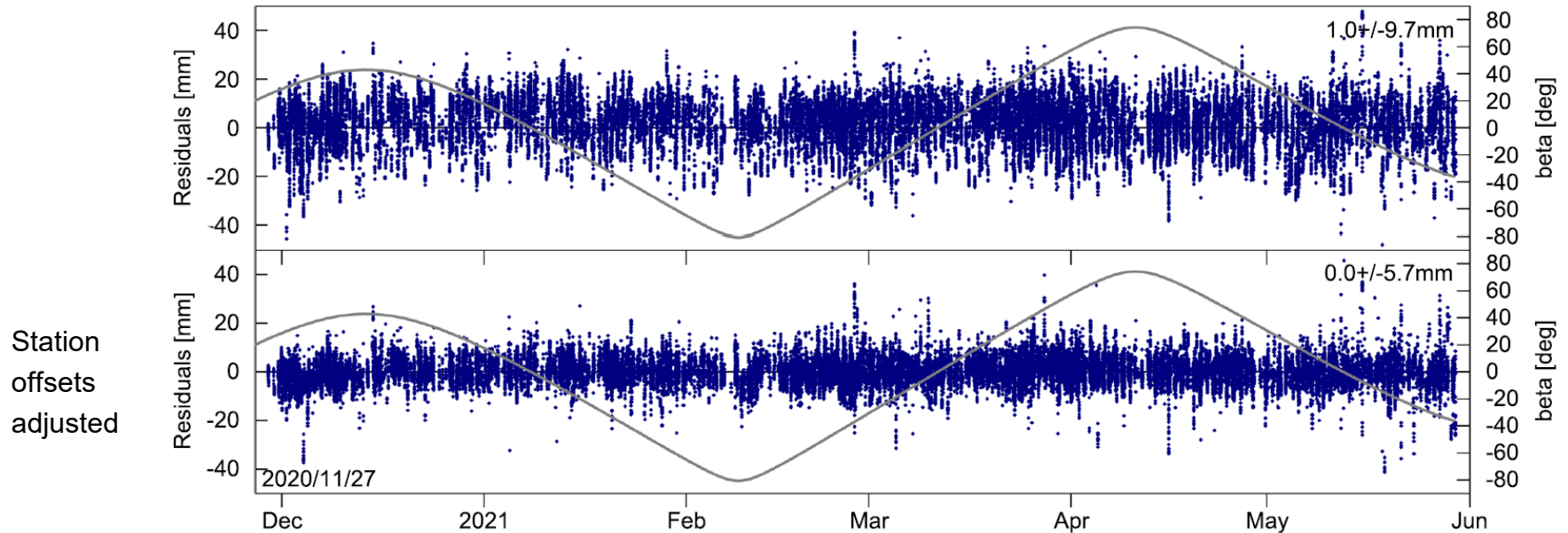
While **Galileo** measurements **exhibit 30–50% smaller RMS errors** than those of GPS, the POD benefits most from the availability of an increased number of satellites. For Sentinel-6A a 1-cm consistency of ambiguity-fixed GPS-only and Galileo-only solutions with the dual-constellation orbits can be demonstrated.

(Montenbruck et al., 2021)

AIUB u^b UNIVERSITÄT BERN
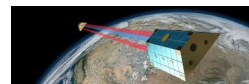
Outlook: GENESIS
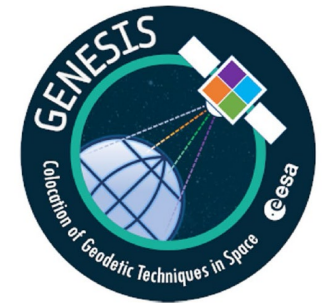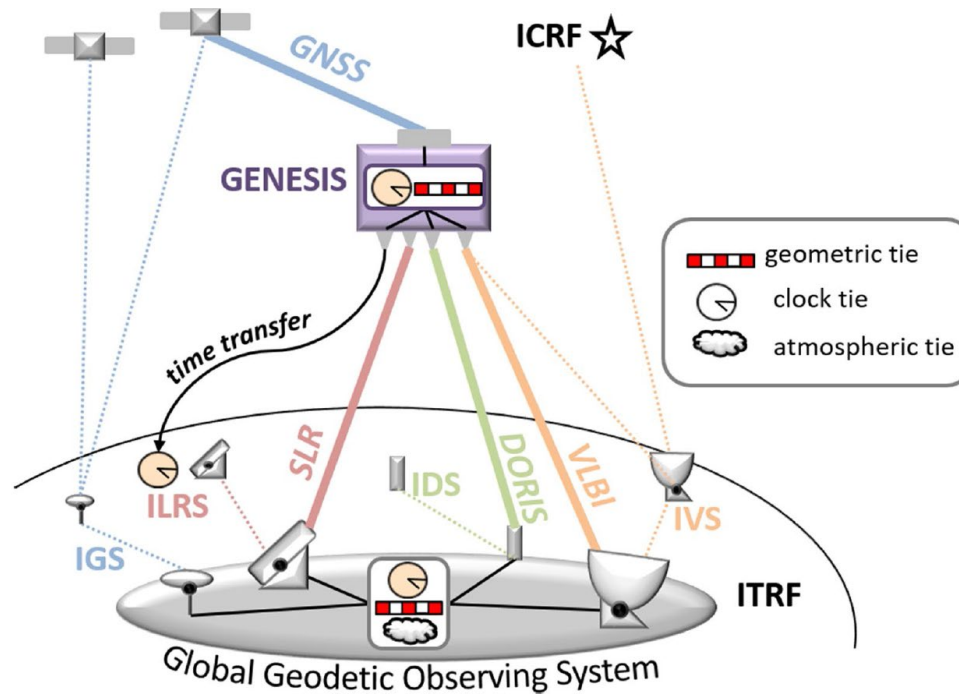
GENESIS will be a dynamic space geodetic observatory carrying all the geodetic instruments referenced to one another through carefully calibrated **space ties**. The co-location of the techniques in space will allow it to determine the Terrestrial Reference Frame (TRF) with **1-mm accuracy** and **0.1 mm/year stability**.

(Delva et al., 2023)

Literature (1)

Arnold, D., A. Jäggi, S. Schaer, C. Kobel, U. Meyer, L. Geisser, O. Montenbruck (2019): Performance of dynamic and ambiguity-fixed LEO orbits in SLR validation and network calibration. OSTST 2019 Meeting, October 21-25, 2019.

Arnold, D., T. Grombein, L. Schreiter, V. Sterken, A. Jäggi (2023): Reprocessed precise science orbits and gravity field recovery for the entire GOCE mission. *Journal of Geodesy*, 97, 67, doi: 10.1007/s00190-023-01752-y

Beutler, G. (2005) Methods of Celestial Mechanics. Vol 1: Physical, Mathematical, and Numerical Principles. Springer, ISBN 3-540-40749-9

Blewitt, G. (1997): Basics of the GPS Technique: Observation Equations, in *Geodetic Applications of GPS*, Swedish Land Survey, pp. 10-54, available at http://www.sbg.ac.at/mat/staff/revers/lectures/2006_2007/GPS/GPSBasics.pdf

Bock, H., R. Dach, A. Jäggi, G. Beutler (2009): High-rate GPS clock corrections from CODE: Support of 1 Hz applications. *Journal of Geodesy*, 83(11), 1083-1094, doi: 10.1007/s00190-009-0326-1

Literature (2)

Bock, H., A. Jäggi, G. Beutler, U. Meyer (2014): GOCE: Precise orbit determination for the entire mission. *Journal of Geodesy*, 88(11), 1047-1060, doi: 10.1007/s00190-014-0742-8

Dach, R., E. Brockmann, S. Schaer, G. Beutler, M. Meindl, L. Prange, H. Bock, A. Jäggi, L. Ostini (2009): GNSS processing at CODE: status report, *Journal of Geodesy*, 83(3-4), 353-366, doi: 10.1007/s00190-008-0281-2

Delva, P., and the GENESIS Science Team (2023): GENESIS: co-location of geodetic techniques in space. *Earth, Planets and Space*, 75, 5, doi: 10.1186/s40623-022-01752-w

Fernández, M., H. Peter, D. Arnold, B. Duan, W. Simons, M. Wermuth, S. Hackel, J. Fernández, A. Jäggi, U. Hugentobler, P. Visser, P. Féménias (2022): Copernicus Sentinel–1 POD Reprocessing Campaign. *Advances in Space Research*, 70(2), 249-267, doi: 10.1016/j.asr.2022.04.036

Grombein, T., M. Lasser, D. Arnold, U. Meyer, A. Jäggi (2022): Determination and Combination of Monthly Gravity Field Time Series from Kinematic Orbits of GRACE, GRACE-FO and Swarm. *IAG Symposia Series,* Vol. 154, 191-201, doi: 10.1007/1345_2022_163
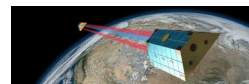
Literature (3)

Jäggi, A., U. Hugentobler, G. Beutler (2006): Pseudo-stochastic orbit modeling techniques for low-Earth satellites. *Journal of Geodesy*, 80(1), 47-60, doi: 10.1007/s00190-006-0029-9

Jäggi, A. (2007): Pseudo-Stochastic Orbit Modeling of Low Earth Satellites Using the Global Positioning System. *Geodätisch-geophysikalische Arbeiten in der Schweiz*, 73, Schweizerische Geodätische Kommission, available at http://www.sgc.ethz.ch/sgc-volumes/sgk-73.pdf

Jäggi, A., R. Dach, O. Montenbruck, U. Hugentobler, H. Bock, G. Beutler (2009): Phase center modeling for LEO GPS receiver antennas and its impact on precise orbit determination. *Journal of Geodesy*, 83(12), 1145-1162, doi: 10.1007/s00190-009-0333-2

Jäggi, A., L. Prange, U. Hugentobler (2011): Impact of covariance information of kinematic positions on orbit reconstruction and gravity field recovery. *Advances in Space Research*, 47(9), 1472-1479, doi: 10.1016/j.asr.2010.12.009

Jäggi, A., H. Bock, U. Meyer, G. Beutler, J. van den IJssel (2015): GOCE: assessment of GPS-only gravity field determination. *Journal of Geodesy*, 89(1), 33-48. doi: 10.1007/s00190-014-0759-z

u^b

UNIVERSITÄT
BERN

AIUB
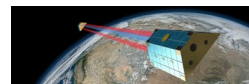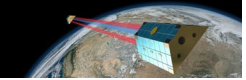
Literature (4)

Jäggi, A., C. Dahle, D. Arnold, H. Bock, U. Meyer, G. Beutler, J. van den IJssel (2016): Swarm kinematic orbits and gravity fields from 18 months of GPS data. *Advances in Space Research*, 57(1), 218-233, doi: 10.1016/j.asr.2015.10.035

Jäggi, A., C. Dahle, D. Arnold, H. Bock, U. Meyer, G. Beutler, J. van den IJssel (2016): Swarm kinematic orbits and gravity fields from 18 months of GPS data. *Advances in Space Research*, 57(1), 218-233, doi: 10.1016/j.asr.2015.10.035

Jäggi, A., D. Arnold, J. Weiss, D. Hunt (2021): Assessment of COSMIC-2 reduced-dynamic and kinematic orbit determination, vEGU21: Gather Online, 19-30 April, 2021

Jäggi, A., H. Peter, D. Arnold, X. Mao (2022): Precise Orbit Determination of the Spire Satellite Constellation for Geodetic, Geophysical, and Ionospheric Applications – Project Overview and First Orbit Determination Results. COSPAR 2022 44th Scientific Assembly, Athens, Greece, 16-24 July, 2022
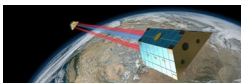
Literature (5)

Lasser, M., U. Meyer, A. Jäggi, T. Mayer-Gürr, A. Kvas, K.H. Neumayer, C. Dahle, F. Flechtner, J.-M. Lemoine, I. Koch, M. Weigelt, J. Flury (2020): Benchmark data for verifying background model implementations in orbit and gravity field determination software. *Advances in Geosciences*, 55, 1-11, doi: 10.5194/adgeo-55-1-2020

Mao, X., D. Arnold, V. Girardin, A. Villiger, A. Jäggi (2021): Dynamic GPS-based LEO orbit determination with 1 cm precision using the Bernese GNSS Software. *Advances in Space Research*, 67(2), 788-805, doi: 10.1016/j.asr.2020.10.012

Mayer-Gürr, T., A. Kvas (2019): COST-G software comparison, Graz University of Technology, benchmark data set available at: ftp://ftp.tugraz.at/outgoing/ITSG/COST-G/softwareComparison/

Montenbruck, O., S. Hackel, A. Jäggi (2018): Precise orbit determination of the Sentinel-3A altimetry satellite using ambiguity-fixed GPS carrier phase observations. *Journal of Geodesy*, 92(7), 711-726, doi: 10.1007/s00190-017-1090-2

AIUB

u^b

UNIVERSITÄT BERN
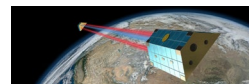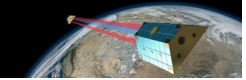
Literature (6)

Montenbruck, O., S. Hackel, M. Wermuth, F. Zangerl (2021): Sentinel-6A precise orbit determination using a combined GPS/Galileo receiver. Journal of Geodesy, 95, 109, doi: 10.1007/s00190-021-01563-z

Peter, H., U. Meyer, M. Lasser, A. Jäggi (2022): COST-G gravity field models for precise orbit determination of Low Earth Orbiting Satellites. Advances in Space Research, 69(12), 4155-4168, doi: 10.1016/j.asr.2022.04.005

Schaer, S., A. Villiger, D. Arnold, R. Dach, L. Prange, A. Jäggi (2021): The CODE ambiguity-fixed clock and phase bias analysis products: generation, properties, and performance. *Journal of Geodesy*, 95, 81, doi: 10.1007/s00190-021-01521-9

Schreiter, L., D. Arnold, V. Sterken, A. Jäggi (2019): Mitigation of ionospheric signatures in Swarm GPS gravity field estimation using weighting strategies. *Annales Geophysicae*, 37, 111-127, doi: 10.5194/angeo-37-111-2019

Svehla, D., M. Rothacher (2004): Kinematic Precise Orbit Determination for Gravity Field Determination, in *A Window on the Future of Geodesy*, edited by F. Sanso, pp. 181-188, Springer, doi: 10.1007/b139065

AIUB

u^b

UNIVERSITÄT
BERN
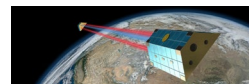
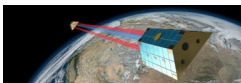# GNSS Background Literature

Teunissen, P.J.G., O. Montenbruck (2017): Springer Handbook of Global Navigation Satellite Systems, Springer, ISBN: 978-3-030-73172-4
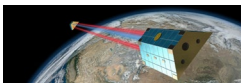
Kinematic LEO Orbit Products (1)

Arnold, D., A. Jäggi (2020): AIUB GRACE kinematic orbits, release 01. Published by Astronomical Institute, University of Bern. http://www.aiub.unibe.ch/download/LEO_ORBITS/GRACE, doi: 10.48350/158372.

Arnold, D., A. Jäggi (2020): AIUB GRACE-FO kinematic orbits, release 01. Published by Astronomical Institute, University of Bern. http://www.aiub.unibe.ch/download/LEO_ORBITS/GRACE-FO, doi: 10.7892/boris.147231.

Arnold, D., A. Jäggi (2020): AIUB Sentinel-1A kinematic orbits, release 01. Published by Astronomical Institute, University of Bern. http://www.aiub.unibe.ch/download/LEO_ORBITS/Sentinel-1A, doi: 10.7892/boris.145822.

Arnold, D., A. Jäggi (2020): AIUB Sentinel-1B kinematic orbits, release 01. Published by Astronomical Institute, University of Bern. http://www.aiub.unibe.ch/download/LEO_ORBITS/Sentinel-1B, doi: 10.7892/boris.145906.
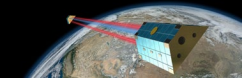
Kinematic LEO Orbit Products (2)

Arnold, D., A. Jäggi (2020): AIUB Sentinel-2A kinematic orbits, release 01. Published by Astronomical Institute, University of Bern. http://www.aiub.unibe.ch/download/LEO_ORBITS/Sentinel-2A, doi: 10.7892/boris.146129.

Arnold, D., A. Jäggi (2020): AIUB Sentinel-2B kinematic orbits, release 01. Published by Astronomical Institute, University of Bern. http://www.aiub.unibe.ch/download/LEO_ORBITS/Sentinel-2B, doi: 10.7892/boris.146133.

Arnold, D., A. Jäggi (2020): AIUB Sentinel-3A kinematic orbits, release 01. Published by Astronomical Institute, University of Bern. http://www.aiub.unibe.ch/download/LEO_ORBITS/Sentinel-3A, doi: 10.7892/boris.147286.

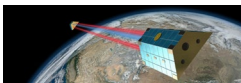Arnold, D., A. Jäggi (2020): AIUB Sentinel-3A kinematic orbits, release 01. Published by Astronomical Institute, University of Bern. http://www.aiub.unibe.ch/download/LEO_ORBITS/Sentinel-3B, doi: 10.7892/boris.147287.
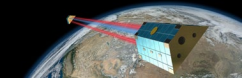
Kinematic LEO Orbit Products (3)

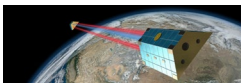Arnold, D., A. Jäggi (2020): AIUB Swarm kinematic orbits, release 03. Published by Astronomical Institute, University of Bern. http://www.aiub.unibe.ch/download/LEO_ORBITS/SWARM, doi: 10.48350/158373.

Pocket Guide of Least-Squares Adjustment (1)

The system of **Observation Equations** is given by:

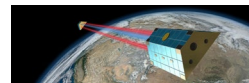$$\boldsymbol{L}' + \boldsymbol{\epsilon} = \boldsymbol{F}(\boldsymbol{X})$$

or, if $\boldsymbol{F}$ is a non-linear function of the parameters, in its **linearized** form:

$$\boldsymbol{L}' + \boldsymbol{\epsilon} = \boldsymbol{F}(\boldsymbol{X}_0) + \boldsymbol{A}\,\boldsymbol{x}$$

$\boldsymbol{L}'$	Tracking observations	$\boldsymbol{X}_0$	A priori parameter values
$\boldsymbol{\epsilon}$	Observation corrections	$\boldsymbol{x}$	Parameter corrections
$\boldsymbol{F}$	Functional model	$\boldsymbol{X}$	Improved parameter values, i.e., $\boldsymbol{X} = \boldsymbol{X}_0 + \boldsymbol{x}$

$$\boldsymbol{A} \doteq \left. \frac{\partial \boldsymbol{F}(\boldsymbol{X})}{\partial \boldsymbol{X}} \right|_{\boldsymbol{X} = \boldsymbol{X}_0} \qquad \text{First design matrix}$$

u^b

UNIVERSITÄT BERN

AIUB

Pocket Guide of Least-Squares Adjustment (2)

The system of **Normal Equations** is obtained by minimizing $\epsilon^T P \epsilon$:
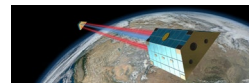
$$\left(A^T P A\right) x - A^T P l = N x - b = 0$$

$N \doteq A^T P A$ \qquad Normal equation matrix

$b \doteq A^T P l$ \qquad Right-hand side with "O-C" term $l \doteq L' - F(X_0)$

$P = \sigma_0^2 C_{ll}^{-1}$ \qquad Weight matrix, from covariance matrix C_{ll} of observations

For a **regular** normal equation matrix the parameter corrections follow as:

$$x = \left(A^T P A\right)^{-1} A^T P l = N^{-1} b$$

AIUB u^b UNIVERSITÄT BERN

Pocket Guide of Least-Squares Adjustment (3)

The **a posteriori standard deviation of unit weight** is computed as:

$$m_0 = \sqrt{\frac{\boldsymbol{\epsilon}^T \, P \, \boldsymbol{\epsilon}}{f}}$$
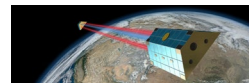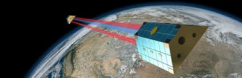
f Degree of freedom (number of observations minus number of parameters)

The **covariance matrix** of the adjusted parameters is given by

$$\boldsymbol{C_{xx}} = m_0^2 \, \boldsymbol{Q_{xx}} = m_0^2 \, \boldsymbol{N}^{-1}$$

and their a posteriori standard deviations follow from the diagonal elements:

$$m_x = \sqrt{C_{xx}} = m_0 \, \sqrt{Q_{xx}}$$

Pocket Guide of Least-Squares Adjustment (4)

Parameter pre-elimination is useful to handle a large number of parameters efficiently. Let us sub-divide the system of normal equations into two parts:

$$\begin{pmatrix} N_{11} & N_{12} \\ N_{21} & N_{22} \end{pmatrix} \cdot \begin{pmatrix} x_1 \\ x_2 \end{pmatrix} = \begin{pmatrix} b_1 \\ b_2 \end{pmatrix}$$

We we may reduce the normal equation system by pre-eliminating epoch-specific parameters x_2 , which yields the modified system of normal equations as

$$N_{11}^* \, x_1 = b_1^*$$

where

$$N_{11}^* = N_{11} - N_{12} \, N_{22}^{-1} \, N_{21}$$ is the normal equation matrix of x_1

$$b_1^* = b_1 - N_{12} \, N_{22}^{-1} \, b_2$$ is the corresponding right-hand side of the normal equation system

$$\frac{u^b}{b}$$ UNIVERSITÄT BERN

AIUB